Mammalian ZAP and KHNYN can independently restrict CpG-enriched avian viruses

Jordan T. Becker[1,5,6], Clayton K. Mickelson[1], Lauren M. Pross[1], Autumn E. Sanders[1], Esther R. Vogt[1], Frances K. Shepherd[1], Chloe Wick[2], Alison J. Barkhymer[1], Stephanie L. Aron[1], Elizabeth J. Fay[1,2], Reuben S. Harris[3,4,5], & Ryan A. Langlois[1,5]

[1]Department of Microbiology and Immunology, University of Minnesota – Twin Cities, Minneapolis, MN, USA, 55455

[2]Department of Biochemistry, Molecular Biology, and Biophysics, University of Minnesota – Twin Cities, Minneapolis, MN, USA, 55455

[3]Department of Biochemistry and Structural Biology, University of Texas Health, San Antonio, TX, USA, 78229

[4]Howard Hughes Medical Institute, University of Texas Health, San Antonio, TX, USA, 78229

[5]Co-corresponding authors

[6]Lead contact

Address correspondence to: beck1169@umn.edu, langlois@umn.edu, or rsh@uthscsa.edu

Short title: ZAP and KHNYN restrict avian viruses

ABSTRACT

Zoonotic viruses are an omnipresent threat to global health. Influenza A virus (IAV) transmits between birds, livestock, and humans. Proviral host factors involved in the cross-species interface are well known. Less is known about antiviral mechanisms that suppress IAV zoonoses. We observed CpG dinucleotide depletion in human IAV relative to avian IAV. Notably, human ZAP selectively depletes CpG-enriched viral RNAs with its cofactor KHNYN. ZAP is conserved in tetrapods but we uncovered that avian species lack KHNYN. We found that chicken ZAP may not affect IAV (PR8) or CpG enriched IAV ($PR8_{CG}$). Human ZAP or KHNYN independently restricted CpG-enriched IAV $PR8_{CG}$ by overexpression in chicken cells and by combined knockout in human cells. Additionally, mammalian ZAP-L and KHNYN also independently restricted an avian retrovirus (ROSV). Curiously, platypus KHNYN, the most divergent from eutherian mammals, was also capable of independent restriction of multiple diverse viruses. We suggest that some mammalian KHNYN can act as a *bona fide* restriction factor with cell-autonomous activity. Furthermore, we speculate that through repeated contact between avian viruses and mammalian hosts, protein changes may accompany CpG-biased mutations or reassortment to evade mammalian ZAP and KHNYN.

INTRODUCTION

Influenza A virus (IAV) is a constantly circulating infectious burden in global waterfowl populations, agricultural animals, and among humans seasonally. Avian IAV occasionally transmits into domesticated mammals and humans. While these infections do not usually result in successful human-to-human spread, they are distinctly pathogenic with a reportedly high mortality rate[1]. However, when novel avian IAV establishes in the human population there can be devastating consequences. Major pandemics have been the result of avian-to-human zoonoses or mixed-animal zoonoses involving avian-swine-human infection chains[2]. Notably, multiple pandemics or large-scale epidemics occurred in 1918, 1957, 1968, and 2009 that resulted in massive infection incidence and mortality in human populations[3]. Much is known about the host dependency factors to which avian IAV must adapt to infect human cells productively[4]. These include differences in viral hemagglutinin binding to host sialic acid linkages[5] with species-specific airway localization[6], pH-sensitivity of viral RNA (vRNA) endosomal release into the cytoplasm[7], and species-specific ability to use the polymerase cofactor, ANP32[8]. Relatively less is known about the network of restriction factors that might specifically target zoonotic IAV infections in mammals[4]. Much of our knowledge of host-pathogen interactions and genetic conflicts has focused on amino acid level and related protein structure changes that predicate animal-to-human adaptation[9]. Comparatively less is known about nucleic acid adaptations driven by host-pathogen conflicts during interspecies infections.

Viral nucleic acid sequence and structure are not only a determinant of protein coding changes, but rather they encompass a complex and sensitive network of features that determine viral fitness, stability, and pathogenesis[10,11]. In addition, host and pathogen genomes are not in equilibrium regarding the frequency and usage of nucleotide doublets[12,13]. For example, CpG dinucleotide frequency is depleted throughout the human genome[14]. Commonly, this is a result of DNA methylation at CpG motifs near promoter sequences that regulate transcription[15]. Mammalian genomes have also selected against encoding CpG dinucleotides in cytoplasmic-resident RNAs[14,16]. Others observed a depletion of CpG content among interferon stimulated genes (ISGs), notably in mammalian species[14,17]. Accordingly, many viral pathogens that infect mammalian species match the dinucleotide content of their host species and mammalian viruses are often CpG-depleted[12,14,18,19]. Others showed that avian IAV sequences exhibit elevated CpG content and that CpG content has depleted over time for IAV strains circulating in humans[14,19]. This suggests that host factors might exist in human hosts to select against CpG-enriched viral nucleic acids that are absent or defective in avian species.

70

71 Recently, several groups showed that the human restriction factor, zinc-finger antiviral protein
72 (ZAP also known as PARP13), specifically binds to and suppresses CpG dinucleotides in
73 cytoplasmic RNA[20,21]. Human ZAP is encoded by the *ZC3HAV1* gene, induced by interferon,
74 and generates multiple isoforms[22,23], including ZAP-L (a 902 amino acid isoform preferentially
75 localized to intracellular membranes) and ZAP-S (a 699 amino acid isoform with diffuse
76 cytoplasmic localization). Like many antiviral proteins, ZAP is evolving under positive
77 selection[24–26]. ZAP antiviral activity is regulated by the interferon-inducible E3 ubiquitin ligase,
78 TRIM25[20,21,27,28]. KHNYN was identified as a ZAP interacting protein and putative cofactor
79 for ZAP antiviral activity[21]. Moreover, KHNYN exhibits basal expression, localizes throughout
80 the cytoplasm[29], and is not interferon-inducible[30]. While KHNYN can exert antiviral effects
81 through ZAP it is unknown if it can exert additional direct antiviral functions. Together, human
82 ZAP, KHNYN, and TRIM25 may function cooperatively, selectively, and/or independently to
83 restrict certain classes of viruses with a bias towards viruses with CpG-enriched nucleotide
84 content[31]. While the function of these human proteins has been well studied, less is known
85 about their non-primate and non-mammalian orthologues and their antiviral restriction ability.

86

87 Understanding the intrinsic and innate immune factors capable of restricting zoonotic viruses is
88 paramount in identifying zoonotic viruses with pandemic potential[32]. Importantly, IAV is a
89 seasonal infectious burden in humans and common zoonosis among wild waterfowl, agricultural
90 birds, domesticated mammals, and humans[4]. We hypothesized that birds might be defective in
91 RNA recognition and restriction pathways and this defect presents a barrier to emergence in
92 mammals. Here, we tested whether restriction factors targeting CpG-enriched RNAs could affect
93 replication of IAV with an elevated CpG-content, mimicking avian IAV. We found that chicken and
94 duck ZAP do not restrict the common laboratory IAV strain (A/Puerto Rico/8/1934/H1N1; PR8)
95 replication regardless of CpG content. We show through genomic, phylogenetic, and functional
96 analyses that multiple avian species may be largely defective in CpG-targeting ZAP function.
97 Additionally, we demonstrate that avian species lack KHNYN, which likely arose through gene
98 duplication after birds and mammals diverged[33,34]. Thus, we used chicken cells as a gain-of-
99 restriction system to test the exogenous provision of host factors for viral restriction. Indeed,
100 human ZAP-S and KHNYN stably expressed in chicken cells independently restricted CpG-
101 enriched PR8 IAV replication. We showed that combined knockout of ZAP and KHNYN in human
102 cells increased replication of CpG-enriched PR8 IAV to a greater extent than single knockout of
103 ZAP or KHNYN alone. We also found that mammalian but not avian (*Galloanserae*) ZAP as well

104 as some mammalian KHNYN proteins can restrict a naturally CpG-enriched avian retrovirus,
105 Rous sarcoma virus (ROSV). Unexpectedly, we discovered a potently antiviral KHNYN
106 homologue from platypus that suggests an ancient restriction pathway. We show that KHNYN
107 may be a *bona fide* restriction factor with cell-autonomous activity. Furthermore, we speculate
108 that through repeated contact between avian and human hosts followed by seasonal circulation
109 among humans, protein level changes for receptor preference and polymerase function could be
110 accompanied by dinucleotide changes and/or CpG-disfavored reassortment that evade restriction
111 by mammalian ZAP and/or KHNYN.
112
113 **RESULTS**
114 **Mammalian IAV sequences are CpG-depleted relative to avian IAV.** Viruses evolve to
115 replicate successfully in their host species. Previous work showed that human IAV exhibited a
116 depletion of CpG dinucleotide content relative to avian IAV sequences since the 1918 IAV
117 pandemic[14,19,35]. Here, surveying influenza sequences in FluDB[36] collected between 1918
118 and 2020, we also observed a depletion of CpG dinucleotides per kilobase (CpG content) in
119 human and swine but not avian IAV sequences over time since 1918 (**S1A Fig**). By comparing all
120 human, swine, and avian IAV segment sequences *en masse*, we observed a lower CpG content
121 in human and swine IAV relative to avian IAV sequences (**Fig 1A**). We observed similar results
122 for ρ_{CG} (rho [ρ] accounts for total C and G content[13,14,17]) but less so for other dinucleotides
123 or %GC content (**S2A-D Fig**). Notably, the largely human-specific influenza B virus[37] (IBV) and
124 influenza C virus[38] (ICV) are CpG-depleted relative to all IAV sequences, speculatively
125 consistent with long-term near-exclusive circulation in mammalian/human populations (**Fig 1A**
126 and **S1-2 Figs**). We observed that human IAV segments 1-3 encoding the heterotrimeric viral
127 polymerase (i.e. PB2, PB1, and PA respectively) are more CpG-depleted relative to avian IAV
128 than segments 4-6 encoding virion proteins (i.e. HA, NP, and NA respectively) typically subject to
129 adaptive immune pressure[39] (**S1B Fig**). We found that when comparing major HA and NA
130 subtypes, CpG content is depleted in subtypes seasonally circulating in humans (H1N1 and
131 H3N2) relative to avian sequences of the same subtype (**S1C Fig**). Conversely, CpG content in
132 human isolates of common avian-to-human zoonotic HA and NA subtypes (e.g. H5N1 and H7N9)
133 is similar to their avian counterparts. The natural history of human IAV includes multiple
134 introductions[40] resulting from avian zoonoses and/or reassortment of avian IAV segments with
135 human viruses in 1918, 1957, 1968, and 2009. We compared CpG content of avian IAV to human
136 IAV during the time periods surrounding the replacement of H1N1 with H2N2 in 1957, H2N2 with
137 H3N2 in 1968, reintroduction of H1N1 in 1977, and pandemic “swine flu” H1N1 in 2009 (**S1D Fig,**

138 **bottom**). We observed that CpG content is lower in human relative to avian IAV sequences during
139 the longer time periods following pandemics in 1977 and 2009 (**S1D Fig, top**). This may reflect
140 periodic reintroduction of CpG-enriched avian sequences that deplete over longer time frames.
141
142 **Chicken and duck ZAP may not restrict replication of CpG-enriched IAV.** We hypothesized
143 that avian species are defective in cytoplasmic CpG-sensing by ZAP and reasoned that this
144 deficiency allows CpG-maintenance of IAV sequences in avian host species. Human ZAP-L and
145 chicken ZAP are homologous proteins encoding four zinc fingers, an inactive poly-ADP-ribose
146 polymerase-like domain[41], and carboxy-terminal prenylation motif[23,29] (**Fig 1B, top**).
147 Previous structural and functional analysis of human ZAP identified zinc finger 2 (ZF2, residues
148 88-110) as responsible for directly recognizing and binding to CpG dinucleotides in the context of
149 short (3-20 nucleotide) and long (full-length 9 kilobase HIV-1 genome) RNA molecules[20,42,43].
150 Using two structural prediction algorithms, we generated models of the four zinc fingers of chicken
151 ZAP (ggaZAP, residues 1-220) by both comparative modeling based on human ZAP (Robetta-
152 CM[44], PDB: 6UEJ[42]) and *ab initio* folding by RoseTTAFold[45] (**S3A-B Fig**). We also
153 compared these structures to the model of chicken ZAP predicted by AlphaFold2[46] (**S3A-B Fig**).
154 As expected, we observed that both *ab initio* predicted structures (RoseTTAFold and AlphaFold2)
155 exhibited lower structural similarity (as measured by root mean squared deviation, RMSD) to
156 human ZAP relative to those generated with comparative modeling (**S3B Fig**). In addition, we
157 observed structural differences between human ZAP and models of duck ZAP as well as quail
158 ZAP (**S3A-B Fig**). Alignment of the amino acid sequences of ZAP homologues revealed multiple
159 amino acid differences between ZF2 of avian and mammalian species (**Fig 1B, bottom**).
160 Therefore, we hypothesized that chicken ZAP is unable to restrict CpG-enriched viruses and
161 tested this hypothesis using the common IAV laboratory strain A/Puerto Rico/8/1934//H1N1 (PR8,
162 blue dashed box) and a CpG-enriched version of PR8[47] ($PR8_{CG}$, orange dashed box; **Fig 1C**).
163
164 In chicken DF-1 cells stably expressing chicken ZAP (ggaZAP) as well as mNeonGreen-tagged
165 chicken ZAP (mNG-ggaZAP), we found no difference in virus replication over 48 hours for PR8
166 or $PR8_{CG}$ relative to vector-transduced (Vector) and mNeonGreen-transduced (mNG) cells (**Fig**
167 **1D**). $PR8_{CG}$ exhibits consistently lower replication relative to wild-type PR8 as previously
168 shown[47] but allows comparisons for viral replication across different cellular contexts. We
169 confirmed expression of transduced proteins by western blot for mNG as well as blasticidin S
170 deaminase (BSD)[48,49] expressed on the bicistronic mRNA and used for drug selection (**S3C**
171 **Fig**). The chicken *ZC3HAV1* gene encodes a single ZAP isoform of 713 amino acids with a

172 carboxy-terminal prenylation motif (amino acids: $_{710}$CIVC$_{713}$) that is homologous to the long
173 isoform of human ZAP (ZAP-L). The short isoform of human ZAP (ZAP-S) is generated by
174 alternative splicing and lacks the carboxy-terminal prenylation motif and the inactive poly-ADP-
175 ribose polymerase-like domain. To test if either prenylation of chicken ZAP or if the divergent ZF2
176 regulate restriction of CpG-enriched PR8 IAV, we generated mutants of chicken ZAP lacking the
177 critical cysteine residue (C710S) for membrane-targeting prenylation, a chimera encoding the
178 human ZF2 (hZF2), or a combination (hZF2.C710S) of these two mutants all of which expressed
179 and localized as expected (**Fig 1E** and **S3D Fig**). However, no form of chicken ZAP restricted
180 PR8 or PR8$_{CG}$ replication (**Fig 1F**). We confirmed protein expression of transduced genes by
181 western blot for mNG as well as BSD (**S3D Fig**). Finally, we found that pooled CRISPR/Cas9-
182 mediated knockout of endogenous ZAP in chicken DF-1 and duck CCL-141 cells had minimal
183 effects on PR8 or PR8$_{CG}$ replication (**Fig 1G-H** and **S4 Fig**). Similarly, we observed that
184 knockdown of endogenous ZAP by stable shRNA in chicken DF-1 cells or transient siRNA in duck
185 CCL-141 cells had minimal effects on PR8 or PR8$_{CG}$ replication (**S3E-G Fig**). qPCR showed
186 endogenous chicken ZAP is expressed in DF-1 cells, induced by interferon, and can be
187 suppressed by shRNA (**S3E Fig**). Attempts at co-expression of human ZAP-S and KHNYN as
188 exogenous transgenes in chicken DF-1 cells were complicated by apparent ZAP-S related
189 inhibition of KHNYN protein expression or stability (**S3H Fig**). Given that human ZAP can use
190 chicken TRIM25 as a cofactor[50], we reasoned that chicken DF-1 cells are potentially deficient
191 in ZAP-dependent antiviral activity targeting this CpG-enriched IAV and could serve as a gain-of-
192 restriction system to test related host factors for the ability to restrict CpG-enriched viruses.
193
194 **Human ZAP-S and KHNYN can independently restrict CpG-enriched PR8 IAV.** Restriction of
195 CpG RNA has been attributed to human ZAP along with its cofactors KHNYN and/or TRIM25.
196 However, we found that avian species may lack a *bona fide* KHNYN orthologue. There are no
197 annotated avian KHNYN orthologues in ensembl, NCBI, or UCSC Genome Browser and a
198 ~400,000bp syntenic region surrounding human KHNYN is missing in avian species, including
199 the KHNYN paralogue – NYNRIN (**S5A Fig**). Human KHNYN and NYNRIN are encoded in
200 tandem on chromosome 14 and NYNRIN is the result of a KHNYN gene duplication and fusion to
201 a retroviral integrase domain[34] (**S5B Fig**). KHNYN and NYNRIN are paralogous to N4BP1[51],
202 a gene conserved in birds, reptiles, and fish (**S5B-C Fig**). We estimated a maximum likelihood
203 phylogeny of human KHNYN, NYNRIN, and N4BP1 orthologues nucleotide sequences from
204 ensembl (**S5C Fig**). We confirmed that N4BP1 is conserved in *Gnathostomats* (i.e. jawed
205 vertebrates including fish, birds, reptiles, and mammals) and is closely related to a fish-specific

206 N4BP1 paralogue (sometimes annotated as *khnyn* or *khnyn-like*, e.g. *Danio rerio khnyn*,
207 ENSDARG00000092488). However, KHNYN found in mammalian species (i.e. monotremes,
208 marsupials, and placentals) and NYNRIN found in therian mammals (i.e. marsupials and
209 placentals) branched together and are more like each other than to the N4BP1 genes (**S5C Fig**).
210 We noted that NCBI and ensembl contain reptile sequences annotated as *KHNYN* (e.g. *Alligator*
211 *mississippiensis KHNYN* XM_014607035.3 or *Anolis carolinensis khnyn*
212 ENSACAG00000009105) that may represent ancestral KHNYN orthologues based on nucleotide
213 sequence (**S5C Fig**; ancient KHNYN orthologues), exon organization, and syntenic neighborhood
214 (**S5D Fig**). Thus, we reasoned that avian species may be defective and/or deficient in two
215 restriction factor genes: ZAP as well as KHNYN. As such, we generated chicken DF-1 cells that
216 stably expressed human ZAP-L, ZAP-S, KHNYN, or TRIM25. We included a mutant of KHNYN
217 that is expected to be enzymatically inactive within its endonuclease domain[21] due to
218 substitution of three critical aspartic acid residues (DDD443/524/525AAA, dKHNYN). We found
219 that ZAP-S as well as KHNYN modestly restricted PR8 relative to vector transduced cells (**Fig**
220 **2A, left**). KHNYN has not been shown previously to act independently of ZAP. Surprisingly, we
221 found that human ZAP-S and KHNYN (but not ZAP-L, dKHNYN, or TRIM25) independently
222 restricted $PR8_{CG}$ relative to vector (**Fig 2A, right**).
223
224 **CpG-targeted restriction requires intact RNA-binding domain of human ZAP and extended**
225 **di-KH domain of KHNYN.** To confirm the role of ZAP-S and KHNYN in restricting $PR8_{CG}$ we
226 generated mutants of each, stably expressed them in DF-1 cells, and performed multicycle IAV
227 replication assays. To test the CpG specificity of ZAP-S in restricting $PR8_{CG}$, we generated a
228 Y108A mutant previously shown to reduce CpG specificity[42] as well as a chimeric human ZAP-
229 S encoding the ZF2 of chicken ZAP (gZF2). Only WT human ZAP-S remained capable of
230 restricting $PR8_{CG}$, an ability that was lost by the Y108A and gZF2 mutants (**Fig 2B**). To test if the
231 prenylation motif (amino acids: CVIS) and corresponding membrane localization of ZAP regulated
232 restriction activity against $PR8_{CG}$, we generated a mutant of ZAP-S that encoded a carboxy-
233 terminal CVIS motif (+CVIS) as well as a C899S mutant of ZAP-L[23]. While the C899S mutant
234 of human ZAP-L did not gain the ability to restrict $PR8_{CG}$, human ZAP-S +CVIS lost the ability to
235 restrict $PR8_{CG}$ as expected (**Fig 2C**). Next, to delineate the manner of KHNYN restriction of $PR8_{CG}$
236 we mutated its extended di-KH domain [52]. KH-domain containing proteins encode a GXXG
237 amino acid motif at the top of a central alpha-helix and mutations in the GXXG motif can reduce
238 RNA-interactions in another KH-domain containing protein, HNRNPK[53]. We generated models
239 of this extended di-KH domain (amino acids 1-213) of KHNYN by *ab initio* folding (RoseTTAFold)

240 (**S5E Fig**) that showed a central alpha-helix with the $_{94}$GAQG$_{97}$ motif at its apex adjacent to a
241 three-helix bundle (**S5E Fig**). This model appeared structurally similar to a recent crystal structure
242 of KHNYN extended di-KH domain[52]. We found that only WT human KHNYN was capable of
243 restricting PR8$_{CG}$ over 48 hours of replication in chicken DF-1 cells but not the catalytically inactive
244 dKHNYN, a AQ95/96DE mutant (AQDE), or a catalytically inactive AQ95/96DE (dAQDE) (**Fig**
245 **2D**). We confirmed expression of transduced human proteins by western blot (**Fig 2E-H**). The
246 Vector transduced cells used in **Fig 1D** showing chicken ZAP had minimal, if any, effects on PR8
247 or PR8$_{CG}$ are the same Vector transduced cells used throughout **Fig 2A-D** showing human ZAP-
248 S and KHNYN restricted PR8$_{CG}$ allowing for relative comparisons in ability for these proteins to
249 restrict these IAV. Nonetheless, we wanted to compare human ZAP-S restriction of PR8 or PR8$_{CG}$
250 to chicken ZAP directly in multicycle IAV replication assays. Using chicken DF-1 cells stably
251 expressing yellow fluorescent protein (YFP) tagged proteins, we found that human ZAP-S and
252 KHNYN restricted PR8$_{CG}$ while human ZAP-L, chicken ZAP, and dKHNYN failed to negatively
253 affect PR8 or PR8$_{CG}$ (**S6A-B Fig**). Human ZAP-S and KHNYN also modestly restricted an avian
254 IAV strain (OH175) with a modest but natural CpG-enriched PA segment (**S6A-C Fig**). Finally,
255 we observed that human ZAP-S, KHNYN, and dKHNYN may independently interact with PR8$_{CG}$
256 segment 5 RNA by RNA immunoprecipitation and quantitative PCR (RIP-qPCR) in infected DF-1
257 cells stably expressing these YFP-tagged proteins (**S6D Fig**). We also observed similar
258 expression of viral proteins (NP) in PR8 and PR8$_{CG}$ infected cells. Together, these results
259 indicated that intact human ZAP-S as well as KHNYN can independently restrict PR8$_{CG}$.
260
261 **Chicken and IAV mRNA are largely unaffected by human ZAP or KHNYN.** To understand
262 how these mammalian restriction factors might affect IAV, we also examined transcriptomic
263 changes during IAV infection. We performed RNA-seq on uninfected as well as PR8 or PR8$_{CG}$
264 infected chicken DF-1 cells stably expressing human ZAP-L, ZAP-S, KHNYN, or dKHNYN to
265 evaluate if these human proteins modulated the chicken transcriptome and viral mRNA
266 expression relative to vector transduced cells. We found that the transcriptomes of uninfected
267 cells were largely unperturbed by whatever human factor was overexpressed (**S7A Fig**)
268 suggesting antiviral activity may not be caused by changing the underlying gene expression
269 profile. Next, we hypothesized that by interacting with and depleting CpG-enriched viral RNAs
270 during multicycle IAV replication experiments, ZAP-S and KHNYN might also negatively bias
271 CpG-enriched segment accumulation during replication. We evaluated relative levels of IAV
272 mRNA segments in PR8 versus PR8$_{CG}$ infected cells in the presence of these different human
273 factors and found similar levels of viral mRNA within segments (**S7B Fig**). Infection with either

274 PR8 or $PR8_{CG}$ resulted in similar gene expression patterns for host cell factors between the two
275 viruses, suggesting that the mechanism of restriction is not through differential induction of host
276 antiviral responses (**S7C Fig**). Together these results suggested initial mechanistic insights into
277 how ZAP and KHNYN might or might not restrict IAV during zoonotic infections in that the
278 restriction may not substantially deplete viral mRNAs.
279
280 **Endogenous human ZAP and KHNYN restrict CpG-enriched viruses.** We next tested the
281 ability of endogenous human ZAP and/or KHNYN to restrict CpG-enriched IAV in human lung
282 cells. Therefore, we generated multiple human lung adenocarcinoma A549 clonal cell lines
283 depleted for ZAP, KHNYN, or both by CRISPR/Cas9 genome editing as well as a vector control
284 (Vector) and a negative control guide targeting *E. coli* LacZ beta-galactosidase (LacZ) clonal cell
285 lines (**Fig 3A-B**). We tested PR8 and $PR8_{CG}$ by multicycle replication assay in these cell lines.
286 We found that single knockout of only ZAP or only KHNYN failed to increase PR8 or $PR8_{CG}$
287 replication relative to LacZ or parental A549 cells (**Fig 3C**). We reasoned that this was consistent
288 with our results by overexpression in DF-1 cells such that either ZAP or KHNYN are capable of
289 independently restricting $PR8_{CG}$. Therefore, we tested multicycle replication of PR8 and $PR8_{CG}$ in
290 double knockout (ZAP and KHNYN depleted, ZK1-2) cells revealing that genetic loss of both ZAP
291 and KHNYN increased replication of $PR8_{CG}$ relative to parental A549 or Vector cell lines (**Fig 3D**)
292 supporting the hypothesis that ZAP and KHNYN can independently restrict of CpG enriched IAV.
293 We tested two single cell clones per gene targeted for knockout to assess potential clonal effects
294 and we hypothesize that the decreased replication in ZAP KO 2 is a clonal effect. The same guide
295 (ZAP guide 2) was used to make the double knockouts that allowed for increased replication
296 across two independent clones. We also found replication of PR8 or $PR8_{CG}$ was unaffected by
297 knockout of endogenous human TRIM25 in A549 cells (**Fig 3E**). Altogether, these results support
298 the hypothesis that ZAP and KHNYN may act independently against CpG-enriched PR8 IAV.
299
300 **ROSV is CpG-enriched and susceptible to mammalian CpG-dependent restriction.** Avian
301 IAV exhibits an enrichment of CpG content relative to human IAV (**Fig 1A, S1-2 Figs**). We next
302 asked if other avian viruses with different levels of human or mammalian zoonotic interactions
303 might exhibit higher levels of CpG enrichment. We noticed that ROSV (a tractable retrovirus
304 model in chicken) exhibits a higher CpG content relative to mammalian retroviruses, including
305 human immunodeficiency virus 1 (HIV-1) or murine leukemia virus (MLV). We observed that
306 ROSV is CpG-enriched along its entire length relative to mammalian retroviruses including HIV-
307 1 or MLV (**Fig 4A**). To determine whether ROSV was subject to CpG-dependent restriction, we

308 performed retroviral assembly and single-cycle infectivity assays (schematic in **Fig 4B**) by co-
309 transfecting chicken DF-1 cells with a full-length ROSV reporter virus expression plasmid and a
310 VSV-G expression plasmid along with increasing amounts of control, human ZAP-L, human ZAP-
311 S, KHNYN, or dKHNYN plasmid. We found that human ZAP-L inhibited ROSV infectivity, but
312 ZAP-S did not (**Fig 4C**). Using mutants of human ZAP-L and ZAP-S, we confirmed that for ROSV,
313 ZAP restriction required an intact ZF2 and prenylation motif (**Fig 4C**). Specifically, the C899S
314 prenylation mutant of ZAP-L failed to restrict ROSV while ZAP-S fused to the four amino acid
315 ZAP-L prenylation motif (+CVIS) gained the ability to restrict ROSV. Next, we tested human ZAP-
316 L, chicken ZAP, and duck ZAP as well as prenylation mutants of each for restriction of ROSV
317 using fusions to mNeongreen. We found that human ZAP-L restricted ROSV but neither of the
318 avian ZAP proteins or their prenylation mutants were much less restrictive (**Fig 4D**). Finally, we
319 tested mammalian orthologues of ZAP from dog, pig, and platypus and found that the prenylated
320 forms of placental mammal ZAP (pig and dog) restricted ROSV, while platypus ZAP or a
321 prenylation mutant (C653S) were less restrictive though they expressed less readily (**S8A Fig**).
322 We confirmed expected subcellular localization of mammalian and avian ZAP isoforms and
323 mutants in chicken DF-1 cells (**S9A Fig**) and observed conservation of CaaX prenylation amino
324 acid motif of representative ZAP orthologues (**S9B Fig**).
325
326 **Mammalian KHNYN restricts ROSV independent of ZAP.** Next, we tested human KHNYN,
327 mutant KHNYN, and mammalian KHNYN orthologues from pig, dog, and platypus for restriction
328 of ROSV. Pigs and dogs are domesticated mammals frequently in contact with agricultural poultry,
329 a common source of avian-to-mammal zoonoses[4]. We selected platypus KHNYN to test
330 because it is the only mammalian species to encode KHNYN but lack the NYNRIN gene[34] (**S3C**
331 **Fig**). We found that pig KHNYN, but not dog KHNYN, similarly restricted ROSV as human KHNYN
332 while platypus KHNYN potently restricted ROSV (**Fig 4E**). We also tested these proteins (with
333 mNeongreen tagged at their amino terminus) relative to catalytically inactivated mutants for ROSV
334 restriction activity (**S8B Fig**). Curiously, mutation of the aspartic acid residues in the NYN
335 endonuclease domains inhibited the restrictive ability for pig KHNYN (DD508/508AA) but not
336 platypus KHNYN (DDD497/498AAA) (**S8B Fig**). We tested multiple truncated forms of platypus
337 KHNYN and found that truncation mutants which fully deleted the endonuclease domain lost
338 restriction activity (**S8C Fig**). We observed that the NYN domains of platypus KHNYN, including
339 the aspartic acid catalytic residues, are relatively well conserved by amino acid alignment and
340 computational structural modeling (**S10A-B Fig**). We generated structural models of platypus
341 KHNYN and noted a substantial structural difference in the loop above the apex of the putative

342 GXXG motif in the KH domain in platypus KHNYN encoding a notably shorter loop relative to
343 human, pig, and dog KHNYN (**S5E Fig**). We confirmed appropriate subcellular localization of
344 these KHNYN orthologues in chicken DF-1 cells (**S10C Fig**). Curiously, we found that platypus
345 KHNYN also restricted HIV-1, a CpG-enriched HIV-1, and MLV, independent of glycoprotein
346 provided for pseudo-typing (**S8D Fig**). We detected cellular expression of retroviral (ROSV
347 Gag^{Pr76} and Gag^{p19}; HIV-1 Gag^{Pr55} and Gag^{p24}; MLV Gag^{mCh}) and antiviral proteins for retroviral
348 assembly and single-cycle infectivity assays as well as loading controls and purified virions from
349 culture supernatants. We noted that platypus KHNYN could potently inhibit virion assembly and
350 release of ROSV, HIV-1, and MLV with typically minimal effects on intracellular Gag expression
351 or loading controls (notably in **Fig 4E** and **S8D Fig**). We also found similar results for mammalian
352 KHNYN restriction of ROSV in the absence of chicken ZAP using DF-1 cells with *ggaZC3HAV1*
353 knocked out by CRISPR/Cas9 (**S8E Fig** and **S4 Fig**). Finally, we tested if platypus KHNYN could
354 restrict IAV replication in human A549 cell lines expressing YFP-tagged platypus KHNYN.
355 Relative to YFP-alone expressing cells, platypus KHNYN modestly inhibited single cycle PR8,
356 pandemic Cal04, and avian-origin OH175 (**Fig 4F**). We also observed that mammalian KHNYN
357 negatively affects viral polymerase activity using an IAV minigenome reporter assay (**Fig 4G**).
358 Together, these results support the hypothesis that mammalian ZAP and KHNYN can restrict
359 CpG-enriched avian viruses, including strains of IAV as well as ROSV. Furthermore, we
360 discovered an orthologue of KHNYN in platypus that may potently restrict multiple viruses from
361 distinct virus families independent of CpG content.
362

363 **DISCUSSION**

364 KHNYN was identified as a ZAP-interacting cofactor that required ZAP to exert a combined
365 antiviral effect against a CpG-enriched HIV-1[21]. Human ZAP functions independent of KHNYN
366 against multiple viruses including HIV-1[20,29,54], Ebolavirus[55,56], Zikavirus[57], and Sindbis
367 virus[28]. Here, we provide the first evidence that KHNYN may be capable of exerting an antiviral
368 effect independent of ZAP. We note that, by definition, restriction factors act in a cell-autonomous
369 fashion[58,59]. Recently, two groups showed that KHNYN binds to RNA through its NYN domain
370 rather than its extended di-KH domain, at least for the substrates tested[52,60]. As such, KHNYN
371 may be a novel *bona fide* restriction factor with incompletely characterized RNA preferences.
372 Furthermore, multiple groups showed different, sometimes conflicting, results regarding ZAP
373 restriction of IAV[61–64]. Here, we observed that human IAV sequences exhibit a marked
374 decrease in CpG content relative to avian IAV sequences (**Fig 1A** and **S1-2 Figs**). We showed
375 that chicken ZAP and duck ZAP may not restrict IAV, in particular PR8 or $PR8_{CG}$ (**Fig 1** and **S3-4**

376 **Figs**) or ROSV (**Figure 4** and **S8 Fig**). We reasoned that chicken cells (e.g. DF-1) could be used
377 as a gain-of-restriction system to test restriction factors for their ability to inhibit IAV and other
378 CpG-enriched viruses. In DF-1 cells stably expressing human ZAP-L, ZAP-S, KHNYN, a
379 catalytically inactive KHNYN, or TRIM25, we found that ZAP-S and KHNYN modestly restricted
380 PR8 and significantly restricted $PR8_{CG}$ (**Fig 2**) Human ZAP-S and KHNYN also restricted an avian
381 strain (OH175) (**S6 Fig**). We also confirmed that this restriction required an intact CpG-
382 recognizing ZF2 of ZAP or a catalytically active KHNYN. We found that human ZAP and KHNYN
383 do not appreciably manipulate the host transcriptome in chicken cells or substantially impact IAV
384 mRNA levels by RNA-seq (**S7 Fig**). We supported our hypothesis that each of these restriction
385 mechanisms can act independently in human cells wherein only combined knockout of both ZAP
386 and KHNYN in human A549 cells increased replication of $PR8_{CG}$ (**Fig 3**). We also found that an
387 avian retrovirus is subject to ZAP and KHNYN restriction, ROSV (**Fig 4** and **S-10 Fig**). Finally, we
388 discovered a potent antiviral KHNYN homologue in platypus capable of restricting multiple
389 divergent retroviruses as well as multiple strains (PR8, $PR8_{CG}$, Cal04, and avian OH175) of IAV
390 (**Fig 4**, **S6 Fig**, and **S8 Fig**). Altogether, we hypothesize that these mammalian restriction factors
391 can act against CpG-enriched viruses including avian viruses and may select for CpG-depleted
392 nucleotide mutations.
393
394 Multiple groups have analyzed the dinucleotide content of influenza sequences, other viruses, as
395 well as host transcripts[12,14,17,19]. Here, we analyzed influenza virus segment sequences from
396 different host species collected over the past century and found the CpG content is depleted over
397 time in mammalian species and that this occurs in polymerase segments more so than HA or NP
398 segments (**Fig 1**). We speculate that over a decades-to-centuries long timeframe, CpG-depletion
399 is a relatively slow adaptative process compared to single amino acid substitutions in PB2, PA,
400 NP, NA, or HA traditionally associated with host species adaptation[65–70]. We observed that
401 H1N1 and H3N2 human IAV sequences exhibited a lower CpG content than subtype-matched
402 avian sequences. However, H5N1 and H7N9 sequences were essentially identical in CpG content
403 between human and avian samples likely reflecting the limited amount of time and replication
404 within human patients. Yet, it is unclear how CpG content regulates viral RNA intrinsic stability or
405 viral replication. Recent work showed that human ZAP targets viral RNA molecules encoding a
406 minimum threshold number of CpG dinucleotides within a length of RNA that is neither too dense
407 nor too sparse[71]. This likely reflects a requirement for some minimum number of ZAP molecules
408 to bind RNA and if CpG dinucleotides are too close these sites occlude each other while if too
409 sparse or too distributed this dilutes a necessary yet undefined minimum of ZAP clustering. Here,

410 we showed that human ZAP-S can target an artificially CpG-enriched PR8 IAV and to a lesser
411 extent PR8 IAV. Future work should examine how CpG number, density (number per length),
412 segment-specificity, and influenza RNA class (viral messenger, complementary, or genomic RNA)
413 are targeted by ZAP perhaps using deep mutational libraries of ZAP zinc fingers and/or target
414 RNAs. Furthermore, we focused on CpG dinucleotides yet other dinucleotide, trinucleotide, or
415 polynucleotide motifs under- or over-represented in host-virus relationships should be examined
416 systematically [72–75]. In addition, much of our knowledge on host-pathogen interactions has
417 focused on Red Queen conflicts highlighted by protein-protein interactions and non-
418 synonymous/synonymous codon (dN/dS) based metrics of positive selection[9,76–79]. Future
419 work should explore other molecular interactions as surfaces for evolutionary conflict (e.g. RNA-
420 protein and RNA-RNA)[80–82].
421
422 Human ZAP-S and ZAP-L can restrict different viruses and human transcripts[83], including those
423 associated with the interferon response[17], based on their differential cellular localization as
424 determined by the carboxy-terminal prenylation motif[23,29,64]. KHNYN was identified by protein-
425 protein interaction with ZAP in a yeast two-hybrid screen and functionally shown to be a required
426 cofactor for ZAP restriction of an artificially CpG-enriched HIV-1 construct[21]. Subsequent work
427 suggested that ZAP-based restriction of different CpG-enriched HIV-1 constructs were not
428 uniformly KHNYN-dependent[54]. Curiously, one group showed that ZAP-L requires the C-
429 terminal prenylation motif to restrict CpG-enriched HIV-1[29] while another found that a C-
430 terminally HA-tagged ZAP-L (that effectively eliminates prenylation) restricted different CpG-
431 enriched HIV-1 mutants[20,50]. It is unclear whether the differences in CpG number and density
432 or other technical differences might explain these differences. Previous work demonstrated that
433 human ZAP-L inhibited IAV (including PR8) by binding viral PB2 and PA proteins but is
434 counteracted by PB1[62]. However, others found that human ZAP-S inhibits IAV (including PR8)
435 by reducing viral mRNA levels but is counteracted by NS1[63]. These two results predated
436 identification of human ZAP preference for CpG dinucleotides. Finally, recent work in human A549
437 cells showed that ZAP-S inhibits PR8 with a CpG-enriched segment 1 but not PR8 with a CpG-
438 enriched segment 5[64]. That virus was not affected by KHNYN KO or TRIM25 KO. In addition,
439 they found that $PR8_{CG}$ (Segment 5) was attenuated in human A549 cells but was not rescued by
440 ZAP KO alone or KHNYN KO alone. They did find that a homo-polymeric stretch of nucleotides
441 in Segment 5 could be mutated to relieve the attenuation of $PR8_{CG}$ in human A549 cells[84].
442 However, combined knockout of ZAP and KHNYN in human A549 cells was not tested. Here, we
443 show that human ZAP-S and KHNYN can independently restrict IAV with a CpG-enriched

444 segment 5 ($PR8_{CG}$; **Fig 2-3**) while ZAP-L and KHNYN can independently restrict ROSV (**Fig 4**).
445 In addition, we found that chicken ZAP was largely ineffective against IAV (PR8, $PR8_{CG}$, or
446 OH175) by over-expression as well as knockout and knockdown (**Fig 1, S3 Fig,** and **S6 Fig**).
447 Knockout and knockdown of duck ZAP similarly failed to affect PR8 or $PR8_{CG}$ replication (**Fig 1**
448 and **S3 Fig**). Previous work showed chicken ZAP was less specific for CpG dinucleotides within
449 the context of human-chicken chimeric proteins[50]. Future work determining the preferred
450 nucleotide preferences of other ZAP orthologues as well as the amino acid, structural, and domain
451 (zinc finger 1-4) determinants of nucleotide preferences will be critical in understanding host-viral
452 ZAP-RNA interactions and evolution. Chicken and duck encode primarily prenylated isoforms of
453 ZAP[85], homologous to ZAP-L. We found that only prenylated isoforms of mammalian ZAP and
454 no forms of chicken or duck ZAP restricted ROSV (**Fig 4** and **S8 Fig**). Curiously, the original
455 discovery of ZAP-dependent restriction of MLV identified and used a form of ZAP lacking the
456 carboxy-terminal prenylation motif[86]. We confirmed that mammalian (human, pig, and dog) and
457 avian (chicken and duck) ZAP proteins localized as expected with long or prenylation motif
458 encoding isoforms at endomembranes and short or prenylation mutants exhibiting diffuse
459 cytoplasmic localization (**S9 Fig**). We also note that platypus ZAP is not particularly restrictive
460 against ROSV and has a more diverse CaaX motif, however mutation of C653S appeared to
461 affect its localization. Future work should explore mammalian ZAP restriction of IAV, in particular
462 common host or mixing vessel species (e.g. pig, cow, or dog).
463
464 KHNYN has not been previously shown to independently restrict any viruses. Here, we discovered
465 platypus KHNYN as a putative potent and broadly acting antiviral restriction factor. However, it is
466 unclear how mammalian KHNYN functions independently to inhibit IAV or ROSV and how
467 platypus KHNYN functions against such diverse viruses. We show preliminary evidence for
468 human KHNYN interaction with IAV $PR8_{CG}$ Segment 5 RNA, yet platypus KHNYN only weakly
469 enriched for this RNA, albeit at lower protein expression levels. In addition, we observed that
470 platypus KHNYN in particular could inhibit the assembly and release of retroviral virions with
471 typically minimal effects on cellular retroviral Gag expression or loading control proteins. We
472 previously showed that artificial relocalization of HIV-1 viral genomic RNA could inhibit virion
473 assembly and release from cells[87,88]. Our results here might suggest platypus KHNYN may
474 accomplish similar inhibition against many retroviruses. We also found that platypus KHNYN
475 could inhibit $PR8_{CG}$ and OH175 in multi-cycle and/or single-cycle IAV assays. It's unclear how or
476 if the antiviral mechanisms of platypus KHNYN against IAV versus retroviruses are similar,
477 related, or distinct. However, many antiviral proteins can exert restriction on viruses through

478 multiple or disparate mechanisms. Notably, APOBEC3 proteins can exhibit both deaminase-
479 dependent and deaminase-independent restriction against multiple viruses[89–92]. In addition,
480 IFITM3 inhibits IAV during virus entry but can inhibit MLV during egress and glycoprotein
481 incorporation into progeny virions[93,94]. We might speculate that platypus KHNYN potency
482 might compensate for platypus ZAP impotency observed in our assays against ROSV. Future
483 work examining their relative antiviral activities and interactions will be informative for
484 understanding the evolution of these two restriction factors. In particular, we showed that platypus
485 KHNYN may exhibit a shorter loop above the extended di-KH domain and future work using
486 chimera or mutants might inform greater molecular details and mechanistic implications of
487 platypus KHNYN antiviral activity. Regardless, platypus KHNYN may function as a *bona fide* cell
488 autonomous restriction factor or potentially use cofactors or cellular features that are conserved
489 across 300 million years of evolution between humans and chickens. Altogether, we suggest that
490 antiviral activities of ZAP and KHNYN might be context dependent. For example, a subset of
491 viruses might be restricted by the membrane-associated ZAP-L and others restricted by the
492 cytosolic ZAP-S because the antiviral activity of many restriction factors is localization-dependent.
493 In addition, ZAP might restrict some sequences, KHNYN might restrict other sequences, and they
494 may act together against yet a third group of sequences. ZAP and KHNYN may also exhibit
495 overlapping and independent restriction preferences as shown in (**Fig 2-3**). In fact, the results
496 from Sharp, et al. suggest mutants of a specific virus strain (e.g. PR8 with CpG-enriched Segment
497 1 versus Segment 5) may exhibit differential susceptibility to ZAP . In the case of segmented
498 viruses, including IAV, this suggests an impact on genetic drift (mutation) as well as genetic shift
499 (reassortment) over time.
500
501 In contrast to ZAP, relatively less is known about the function, preferences, and regulation of
502 KHNYN. KHNYN is one member of family of paralogous genes encoding a putative RNA-binding
503 domain fused to a NYN-endonuclease domain[51]. Our phylogenetic analysis (**S5 Fig**) support
504 the hypothesis and previous reports that KHNYN may be derived from N4BP1 occurring prior to
505 the radiation of mammalian species and NYNRIN is the result of a gene duplication and
506 fusion/integration of KHNYN to Metaviral *Pol* gene occurring between the emergence of
507 monotreme and therian mammals[34]. We showed here that mutation of key aspartic acid
508 residues in the NYN domain of KHNYN reduce its restriction ability, similar to others[21]. We also
509 show that mutations in the KH-domain of KHNYN reduces its restriction ability[53]. Recent
510 structural and biochemical studies showed the extended di-KH domain of KHNYN does not bind
511 RNA but the full-length KHNYN protein binds RNA without CpG preferences and the NYN domain

512 exhibits single-stranded endonuclease specificity[60]. Furthermore, how these preferences and
513 activity change over evolutionary time is unclear. Finally, while we identified serendipitously the
514 potent platypus KHNYN restriction factor, its mechanism of action is unclear. We speculate that
515 this potent ancestral KHNYN required attenuation for the genesis of retroelement-derived
516 NYNRIN and retroviral-associated placentation acquired during the rapid evolutionary leap from
517 monotremes to therian mammals between 180-160 million years ago[34,95].
518
519 **LIMITATIONS**
520 We appreciate limitations exist in this study attempting to synthesize and understand the multiple
521 (and sometimes conflicting) reports regarding CpG-depletion in cytoplasmic-resident RNAs and
522 viral adaptation driven by ZAP, KHNYN, and related antiviral genes. Throughout this study we
523 primarily use a common laboratory strain of IAV and a previously published CpG-enriched
524 segment 5 mutant strain (PR8 and $PR8_{CG}$) as well as in some assays an avian strain (OH175)
525 and human pandemic strain (Cal04). Future work will benefit from examining ZAP, KHNYN, and
526 TRIM25 susceptibility of many influenza strains derived from humans, wild birds, agricultural
527 poultry, and domestic mammals as well as emerging mammalian H5N1 IAV isolates[96]. This
528 work largely uses chicken cell lines and relies on overexpression of many host restriction factors
529 by transfection or stable transduction. While aspects of our work were substantiated by
530 knockdown and/or knockout of endogenous host cell factors, future work will benefit from using
531 primary cells[97]. Furthermore, future work will also benefit from cell systems derived from avian
532 reservoir species including shorebirds that currently do not exist as tractable laboratory models.
533 We attempted to build chicken DF-1 cells constitutively expressing both ZAP and KHNYN using
534 native human CDS. Future work may benefit from codon-optimized and inducible expression
535 systems compared across different host species. Finally, we acknowledge two aspects of
536 KHNYN antiviral activity shown here are limited. Specifically, the mechanisms of KHNYN antiviral
537 activity should be fully elucidated in the future including potential co-factors. Curiously, we found
538 platypus KHNYN potently active in chicken DF-1 cells and human HEK293T cells suggesting
539 either a conserved co-factor or cell-autonomous restriction factor activity. Many restriction factors
540 exhibit cell-autonomous activity. Human and mouse APOBEC3 proteins function almost
541 universally in vertebrate cell lines against retroviruses as well as in yeast against many Ty3
542 retrotransposons[98]. Similarly, human TETHERIN restricts avian leukosis viruses when
543 expressed in chicken cells and chicken TETHERIN restricts HIV-1 when expressed in human
544 cells[99]. Future work should examine what cofactors, proteins, and/or RNA molecules
545 interact[100] with mammalian and avian ZAP as well as mammalian KHNYN across different

546 cellular contexts and their impact on antiviral activity. In addition, the potent antiviral platypus
547 KHNYN orthologue is derived from a predicted mRNA and protein product and investigation of its
548 mechanism of action will be vastly informative. However, the sum of the results shown here should
549 spur multiple important research directions and warrant intense interest in multiple fields including
550 host-pathogen interactions, virus evolution, mammalian evolution, and embryonic development.

551 **METHODS**

552

553 **Cell lines.** Mammalian cells, chicken DF-1 cells, and duck CCL-141 cells were grown in DMEM
554 supplemented with 10% fetal bovine serum (FBS) and 1% penicillin/streptomycin. Chicken DT40
555 cells were grown in DMEM supplemented with 10% FBS, 10% tryptose phosphate buffer, 1%
556 penicillin/streptomycin, and 50μM beta-mercaptomethanol. Cells were maintained at 37°C, 5%
557 CO_2, and 50% humidity. HEK293T (male human epithelial kidney, ATCC, CRL-3216), A549 (male
558 human lung carcinoma, ATCC, CCL-185), PK-15 (male porcine kidney, ATCC, CCL-33), MDCK
559 (female canine kidney, ATCC, CCL-34), DF-1 (unspecified sex chicken embryonic fibroblast,
560 ATCC, CRL-12203), DT40 (unspecified sex chicken lymphoblast, ATCC, CRL-2111), and CCL-
561 141 (unspecified sex duck embryonic fibroblast, ATCC) cells were obtained from ATCC and used
562 without extensive passaging. Sup-T11 (male human T lymphoblast clone derived from Sup-T1,
563 ATCC, CRL-1942) cells have been described previously[101].

564

565 **Plasmids.** A CpG-enriched IAV segment 5 (encoding nucleoprotein, NP) derived from Gaunt, et
566 al.[47], ordered from IDT as a gBlock, and cloned into a pDZ bidirectional influenza vRNA/mRNA
567 expression plasmid[102] via In-Fusion (Takara Bio). Expression plasmids for human ZAP-L, ZAP-
568 S, KHNYN, and TRIM25 as well as pig ZAP, chicken ZAP, and pig KHNYN were generated using
569 conventional molecular biology techniques. Specifically, RNA was extracted from human A549
570 cells, chicken DF-1, or pig PK15 cells using Qiagen RNeasy Mini Kit, cDNA synthesized using
571 QIAGEN Quantitect cDNA Synthesis Kit, and genes of interest were amplified by PCR from first-
572 strand cDNA, restriction enzyme digested, and ligated into bespoke MLV-based retroviral vectors
573 also harboring blasticidin S deaminase (BSD) or hygromycin resistance genes downstream of an
574 IRES for bicistronic expression[100,103,104] or bespoke pcDNA3-based expression vectors. Dog
575 and platypus KHNYN as well as dog and platypus ZAP were ordered from IDT as gBlocks. Duck
576 ZAP was synthesized by Twist Biosciences followed by subcloning into additional plasmid
577 backbones. Mutants, chimeras, and fluorescently tagged versions of all plasmids were generated
578 by site-directed mutagenesis and/or overlapping PCR and subcloned into expression vectors
579 using Phusion DNA polymerase and T4 DNA ligase (NEB). RCAS-GFP plasmid[105] was a gift
580 of Connie Cepko (Addgene #13878). ROSV-mCherry was generated by replacing EGFP in
581 RCAS-GFP with mCherry followed by site-directed mutagenesis to inactivate the Env glycoprotein
582 open reading reframe. HIV-mCherry has been described previously[87]. HIV_{CG}-mCh was cloned
583 by inserting a gBlock (IDT) encoding env86-561CpG[21] (from NCBI: MN685350.1[21]) into an
584 HIV-1 NL4-3 Env- Vpr- Nef- mCherry+ (HIV-mCh) reporter virus expression plasmid. MLV-Gag-

585 HA-mCh was a kind gift of Nathan Sherer[106]. Codon-optimized HIV-1 NL4-3 Env (SynEnv) was
586 synthesized as a gBlock by IDT prior to subcloning into pcDNA3.2. pCAG-RABV-G (Addgene
587 #36398) expressing Rabies virus glycoprotein (RABV-G) was a kind gift of Connie Cepko[107].
588 CRISPR/Cas9 editing of human A549 cells was performed by lentiviral transduction using
589 pLentiCRISPR1000[108]. Attempts at genetic editing in avian cells with pLentiCRISPR1000 were
590 unsuccessful. CRISPR/Cas9 editing of avian cells was performed by sequential retroviral
591 transduction of Cas9-GFP expression vector followed by single guide RNA (sgRNA) expression
592 vector – both bespoke plasmids generated for this study. Briefly, guide RNAs were designed from
593 the literature, Synthego design tool, or RGEN Cas-Designer[109], complementary oligos with
594 Esp3I restriction enzyme compatible ends were annealed, and subsequently ligated into
595 pLentiCRISPR1000 or pMLV.miRFP670.iU6sgRNA via Golden-Gate ligation with T4 DNA ligase.
596 IAV bidirectional rescue plasmids (pDZ) have been described previously[110]. Lentiviral
597 constructs for shRNA knockdown of chicken ZAP were cloned by annealing complementary oligos
598 with AgeI and EcoRI restriction enzyme compatible ends and subsequently ligated into pLKO.2
599 via Golden-Gate ligation with T4 DNA ligase. shRNAs were designed targeting chicken ZC3HAV1
600 using the Broad Institute's Genetic Perturbation Platform[111]. DNA constructs were sequence
601 confirmed by whole plasmid sequencing performed by Plasmidsaurus using Oxford Nanopore
602 Technology or Sanger sequencing performed by Eurofins Scientific or GeneWiz from Azenta.
603 Plasmid, shRNA, siRNA, and sgRNA sequences are provided in **S1 Table**.
604
605 **Retroviral transductions and stable cell generation.** Simple retroviruses for transduction were
606 generated by transfecting HEK293T cells with 1µg vector plasmid[100,104], 1µg pMD-
607 gagpol[112], and 200ng pMD-VSVG[113] using Transit-LT1 (Mirus Bio), changing media after 24
608 hours, and harvesting culture supernatant at 48 hours post-transfection followed by 0.45µm
609 syringe filtration. Lentiviruses for transduction were generated by transfecting HEK293T with
610 1.25µg pLentiCRISPR1000 or pLKO.2_shRNA plasmid, 750ng psPAX2 (Addgene plasmid
611 #12260; encoding Gag/GagPol, Rev, Tat), and 200ng pMD-VSVG, changing media after 24
612 hours, and harvesting culture supernatant at 48 hours post-transfection followed by 0.45µm
613 syringe filtration. Transducing virus preps were aliquoted and stored at -20°C. Stable cells were
614 generated as previously described[87,114]. Briefly, approximately 2500 target cells were seeded
615 into a 96-well flat bottom plate, allowed to adhere overnight, and 20-200µL of transducing viral
616 supernatant with up to 10µg/mL polybrene added to each well. After 2-3 days in culture,
617 transduced cells are washed with PBS, and fresh media containing antibiotic (2µg/mL puromycin,
618 2µg/mL blasticidin, or 200µg/mL hygromycin; GoldBio, Inc) added. Cells were grown and

619 expanded in the ongoing presence of antibiotic. In the case of CRISPR/Cas9 lentiviral
620 transduction, A549 cells were single cell cloned by serial dilution (re-plating from pooled
621 transducing culture as above into 96-well flat bottom plates at 25, 5, 1, and 0.2 cells per well or
622 by gradient dilution down and across 96-well plates). After 2-4 days, single cell-derived colonies
623 were marked and followed regularly, expanded, and then screened initially by western blot or
624 PCR. Multiple independent clones were screened for each knockout. Genetic knockout in A549
625 cells was confirmed by western blot or genomic DNA extraction, amplification of Cas9 target site,
626 blunt cloning into pJET1.2 (Thermo Scientific), and Sanger sequencing multiple transformed
627 clones. Double knockout cells were transduced simultaneously (A549.ZK1 and A549.ZK2) with
628 ZAP-targeting (blasticidin-resistant) and KHNYN-targeting (puromycin-resistant) CRISPR/Cas9
629 lentiviruses, selected with both antibiotics after 48 hours, single cell cloned, screened by western
630 blot or PCR, and confirmed by Sanger sequencing. Avian cells were transduced with simple
631 retrovirus Cas9-GFP (puromycin-resistant). Avian cell knockouts were maintained as pools stably
632 expressing Cas9 and sgRNAs (blasticidin-resistant). Genetic knockout in avian cells was
633 determined by genomic DNA extraction, PCR amplification of Cas9 target site, Sanger
634 sequencing of pooled amplicons, and computational deconvolution of overlapping
635 chromatograms by TIDE analysis[115].
636
637 **Influenza viruses.** Wild-type Influenza A/Puerto Rico/8/1934(H1N1) (PR8) was rescued by
638 plasmid-based transfection into HEK293T cells using Lipofectamine 3000 (ThermoFisher
639 Scientific) and amplified in 10-day old embryonated chicken eggs. $PR8_{CG}$ virus was made by
640 plasmid-based transfection with the WT segment 5 plasmid replaced with CpG-enriched segment
641 5 and amplified in embryonated chicken eggs. Single-cycle PR8 and Cal04
642 (A/California/04/2009(H1N1)) that lack virus-encoded HA and instead express mCherry from the
643 HA segment were rescued by plasmid-based transfection into HEK293T cells and amplified in
644 MDCK cells stably expressing PR8 HA[116]. Chimeric OH175 Influenza A/Green-Winged
645 Teal/Ohio/175/1986(H2N1) viruses[67] were rescued by plasmid-based transfection into
646 HEK293T cells using six internal segment plasmids from OH175 as well as the HA and NA
647 segment plasmids from PR8 for biosafety reasons and subsequently amplified in MDCK cells.
648 PR8, $PR8_{CG}$, and OH175 transfections were performed in combination with pCAGGS expression
649 plasmids as needed. OH175 plasmids (also known as S009) were a kind gift of Andrew Mehle.
650 Viral titers were determined by plaque assay in MDCK cells as previously described[117].
651

652 **Influenza multicycle replication assays.** For multicycle IAV infections, 500,000 A549 or DF-1
653 cells were plated in 6-well plates (or 100,000 CCL-141 in 12-well) and allowed to grow overnight
654 for up to 24 hours. Cells were infected at an MOI of 0.05 infecting a confluent culture of cells, as
655 previously described[117]. For each cell condition (e.g. DF-1 Vector, ZAP, KHNYN) and for each
656 virus (e.g. PR8 or $PR8_{CG}$) there were three independently infected well replicates (with the
657 exception of multicycle replication assays in **S6A Fig** using two independently infected well
658 replicates). Briefly, cells were washed with PBS prior to addition of 1mL infection media (1x PBS,
659 2.5% bovine serum albumin, 1% calcium/magnesium). Viral stocks were diluted such that 40µL
660 of inoculum could be added to each well yielding an MOI of 0.05 plaque forming units per cell
661 (pfu/cell). After addition of viral inoculum, cells were incubated at 37°C for 1 hour. Next, cells were
662 washed with PBS prior to addition of 2.5mL viral growth medium (1x DMEM, 2.5% HEPES buffer,
663 2.5% bovine serum fraction V [7.5%], 1% penicillin/streptomycin) supplemented with TPCK-
664 resistant trypsin (1µg/mL for A549 as well as 0.625 µg/mL for DF-1 and CCL-141). Culture
665 supernatants (at least two aliquots of 200µL each) were collected immediately after addition to
666 wells (0 hours post-infection) and at 24- and 48-hours post-infection (hpi) and optionally at 12-
667 hours post-infection. Supernatants were stored at -80°C until viral titer was determined by plaque
668 assay in MDCK cells as previously described[117]. Multicycle replication assays were performed
669 in triplicate with key results being replicated in independent assays (e.g. ZAP-S relative to Vector
670 in **Fig 2A, 2B, and 2C**). Plaque assays were performed and quantified single-blinded. For
671 transient knockdown by siRNA, 100,000 CCL-141 cells were plate in 12-well plates and
672 transfected with mock, 5nM scramble control, and 1nM or 10nM pools of 10 duplex siRNAs
673 targeting *Anas platyrhynchus* ZC3HAV1 (aplZAP) using RNAiMAX (ThermoFisher). siRNAs were
674 designed using IDT dsiRNA design tool and sequences are provided in **S1 Table**.
675
676 **Single-cycle retrovirus assembly and infectivity assay.** For ROSV, 500,000 DF-1 cells were
677 plated into 6-well plates in 2mL media, cultured overnight, and transfected with 1.6µg RCAS-
678 mCherry, 200ng pMD-VSVG, 100/200/400ng gene of interest plasmid, and topped up to 2.2µg
679 total plasmid DNA mass with pBlueScript using TransIT-LT1 (Mirus Bio). At 24 hours post-
680 transfection, we exchanged media. At 48 hours post-transfection, virus-containing supernatants
681 were harvested and filtered using 3mL syringes and 0.45µm syringe PVDF filters. Transfections
682 were performed as dose-titrations of gene of interest plasmid amounts rather than triplicates of a
683 single plasmid amount. Culture supernatants were used to infect chicken DT40 suspension cells
684 in triplicate and the remaining volume was stored at -80°C. We performed flow cytometry to detect
685 infected (i.e. % mCherry-positive) DT40 cells at 48 hours post-infection using a Becton Dickinson

686 FACS Canto II with a high-throughput plate-based sample aspirator. For MLV, HEK293T cells
687 were plated and transfected with 500ng pMD-gagpol, 1100ng pMLV-Gag-HA-mCherry, 200ng
688 pMD-VSVG, 100/200/400ng gene of interest plasmid, and topped up to 2.2µg total plasmid DNA
689 mass with pBlueScript. For HIV-1, HEK293T cells were plated and transfected with 1600ng pHIV-
690 mCherry, 200ng glycoprotein-expression plasmid (pMD2-VSVG, pCAG-RABVG, or
691 pcDNA.HIV.SynEnv), 100/200/400ng gene of interest plasmid, and topped up to 2.2µg total
692 plasmid DNA mass with pBlueScript. MLV single-cycle infectivity was detected by infecting
693 HEK239T cells and HIV-1 infectivity was detected using SupT11 cells (for VSV-G and HIV Env
694 pseudo-typed virus) or HEK293T cells (for RABV-G pseudo-typed virus).
695
696 **Western blotting and antibodies.** A549 cells were treated with 1000U/mL of universal
697 interferon-alpha (PBL Assay Sciences, #11200-2) for 24 hours prior to pelleting cells and lysing
698 in 2.5X reducing sample buffer (RSB; 125 mM Tris HCl, 20% glycerol, 7.5% SDS, 5% β-
699 mercaptoethanol, 250 mM DTT, 0.05% Orange G, pH 6.8), and boiled at 98°C for 15 minutes
700 prior to storage at -80°C. Transfected DF-1 and HEK293T cells for single-cycle retrovirus
701 assembly assays were harvested at 48 hours post-transfections, pelleted by centrifugation, lysed
702 in 2.5X reducing sample buffer (RSB), and boiled at 98°C for 15 minutes prior to storage at -80°C.
703 Virus-containing supernatants (1mL) from retrovirus assays were underlaid with 200µL of 20%
704 sucrose (diluted in 1X PBS), centrifugated at ≥21,500g for two hours at 4°C, liquid aspirated, and
705 pellet resuspended in 2.5X RSB. Western blots were performed conventionally using commercial
706 precast polyacrylamide gels (26-well Bio-Rad, 4-20% Criterion TGX, #5671095) for
707 electrophoresis (60 volts for 60 minutes followed by 120 volts for 60 minutes) and transferred to
708 0.2µm nitrocellulose membrane using Invitrogen Power Blotter XL (ThermoFisher Scientific; ≤25
709 volts). Membranes were washed in PBS and PBST (PBS with 0.1% Tween-20) followed by
710 blocking (2% dry milk in PBST). With constant rocking at all steps, membranes were incubated
711 with primary antibodies overnight at 4°C, followed by three washes for five minutes each with
712 PBST, incubation with secondary antibodies in 2% milk in PBST for at least one hour at room
713 temperature, followed by three washes for five minutes each in PBST, and one final wash in PBS.
714 Primary antibodies used at indicated dilutions are provided in **S1 Table**. Secondary antibodies
715 used include goat anti-mouse IgG IRDye 680LT and goat anti-rabbit IgG IRDye 800CW (both
716 used at 1:10,000 dilution in 2% milk in PBST). Membranes were imaged using a LiCor Odyssey
717 Fc infrared fluorescent imager for two or 10 minutes per channel.
718

719 **GFP-Trap immunoprecipitation.** Chicken DF-1 cells including those stably expressing YFP-
720 tagged ZAP and KHNYN orthologues were infected with PR8 and $PR8_{CG}$ at MOI=5 as described
721 above in 10cm dishes and harvested at 24 hours post-infection. A portion of each sample set
722 aside for 10% input RNA (with RNase Inhibitor) and 10% input protein (resuspended in RSB and
723 boiled) then stored at -80°C. Remaining cells were washed twice with cold 1X PBS (containing
724 RNase inhibitor) and resuspended in radioimmunoprecipitation assay buffer (RIPA: 10mM Tris-
725 HCl, 150mM NaCl, 0.5mM EDTA, 0.1% SDS, 1% Triton-X, 1% sodium deoxycholate, 2.5mM
726 $MgCl_2$, 1mM phenylmethylsulfonyl fluoride, 1 unit/mL DNaseI, and 1 unit/mL RNase Inhibitor
727 (Roche, #3335399001). Samples were needle-lysed with a 26G needle, slowly inverted
728 continuously at 4°C for 30 minutes, and centrifugated at ≥21,500g for 10 minutes at 4°C. GFP-
729 Trap agarose beads (ProteinTech, #gta) were equilibrated in dilution buffer (10mM Tris-HCl,
730 150mM NaCl, 0.5mM EDTA) with 50µL bead slurry per sample into 500µL dilution buffer per
731 sample. Beads were centrifugated at 2500g for 5 minutes at 4°C and washed with dilution buffer
732 twice more. Remaining RIPA supernatant of each sample was added to 500µL of equilibrated
733 beads in dilution buffer and slowly inverted continuously at 4°C overnight. Beads were
734 centrifugated at 2500g for 5 minutes at 4°C and resuspended in wash buffer (10mM Tris-HCl,
735 150mM NaCl, 0.5mM EDTA, 0.05% IGEPAL) twice and then split into two equivalent volume
736 samples. One subjected to RNA extraction by Qiagen RNeasy Kit. The other centrifugated once
737 more, supernatant aspirated, bead pellet resuspended in RSB, boiled at 98°C for 15 minutes, and
738 stored at -80°C.
739
740 **Fluorescence microscopy.** Fixed-cell images were obtained on a BioTek Cytation 5 (Agilent)
741 using a 4X (NA=0.13, #1220519), 20X (NA=0.40, #1220517), or 40X (NA=0.6, #1220544) Plan
742 Fluorite objective and LED-filter cube sets for DAPI (excitation = 377±50nm; emission =
743 447±60nm; #1225007 and #1225100), GFP for mNeonGreen (excitation = 469±35; emission =
744 525±39; #1225001 and #1225101), and TRITC for mCherry and AlexaFluor568 (excitation =
745 556±29; emission = 600±37; #1225012 and #1225125). We quantified single-cycle IAV infections
746 by imaging and used the BioTek Gen5 software to calculate percent infectivity using scPR8
747 (MOI=5) and scCal04 (MOI=5) encoded mCherry as a readout for infectivity (# TRITC+ cells / #
748 DAPI-stained nuclei). To quantify OH175 non-replicating infections, we performed
749 immunofluorescence on infected cells (MOI=0.5 without TPCK trypsin to block virus transmission)
750 fixed with 4% paraformaldehyde at 24 hours post-infection. Briefly, we subjected cells to
751 permeabilization (PBS with 0.25% Triton X-100) for 10 minutes, blocking (PBS with 3% bovine
752 serum albumin), primary antibody staining with mouse anti-NP (BEI, NR-43899, 1:500) in blocking

753 buffer (3% bovine serum albumin) for one hour, secondary antibody staining with goat anti-rabbit
754 AlexaFlour-568 (Invitrogen, #A-11031, 1:500), and nuclear counterstaining with DAPI (Sigma,
755 D9542, 100ng/mL).
756
757 **Minigenome reporter assay.** Chicken DF-1 cells were seeded into 96-well glass bottom plates,
758 allowed to adhere overnight, and then transfected with equal amounts of plasmids encoding IAV
759 heterotrimeric polymerase (pCAGGS.PB2, pCAGGS.PB1, and pCAGGS.PA), wild-type IAV NP
760 (pCAGGS.NP), and a vRNA/negative-sense IAV-codon-optimized mCherry expression plasmid
761 (pPol.mCherry) [118] as well as plasmids encoding mNeongreen or mNeongreen-tagged
762 mammalian KHNYN orthologues with TransIT-LT1. At 24 hours, cells were washed with 1X PBS,
763 fixed with 4% paraformaldehyde, counterstained with DAPI, and imaged for mNeongreen and
764 mCherry expression as a % mCherry-positive as described above.
765
766 **Structural models of ZAP and KHNYN.** For structural models of ZAP, amino acid sequences
767 for the four zinc finger domains of different species and mutants of ZAP were used as input for
768 RobettaCM using the human ZAP crystal structure (PDB: 6UEJ) for comparative modeling. We
769 noted that in most cases, *ab initio* folding by AlphaFold or RoseTTAFold may not capture metal
770 ion-coordinated finger structures. Sequences used are provided in **S1 Table**. Models generated
771 and 6UEJ are shown in **S1 Data**. For structural models of KHNYN, amino acid sequences for the
772 KH domain or NYN domain of KHNYN were used as input for RoseTTAFold using default settings.
773 Sequences used are shown in **S1 Table**. Both RoseTTAFold and RobettaCM are publicly
774 available at robetta.bakerlab.org. All models generated are provided in **S2-3 Data**. Models were
775 visualized in Chimera (v1.13.1, build 41965, UCSC) and aligned using MatchMaker with a
776 Needleman-Wunsch alignment algorithm and BLOSUM-62 matrix.
777
778 **Phylogenetic analyses.** Coding sequences (CDS) of human KHNYN, NYNRIN, N4BP1, and
779 their orthologues were downloaded from ensembl. CDS of ZAP homologues were downloaded
780 from ensembl. CDS were aligned using ClustalOmega in Seaview (V5.0.4). Phylogenetic trees
781 were generated in Seaview using PhyML with 100 bootstraps using CDS. Synteny schematics
782 were generated manually in Adobe Illustrator using data from UCSC ENCODE Genome Browser,
783 NCBI, and ensembl. Alignments and phylogenetic trees are available in **S4-5 Data**.
784
785 **Virus bioinformatic analysis.** Full-length influenza virus sequences were downloaded from the
786 Influenza Research Database for each animal host species (human A, avian A, swine A, human

787 B, and human C) including the nucleotide sequence, host, collection date, and subtype.
788 Dinucleotide values were counted by string count. Data were plotted using ggplot2. Data are
789 available at a zenodo record (doi: 10.5281/zenodo.14919910) and R code is available in **S1 File**.
790 Sliding window CpG data were analyzed using an in-house custom script (cpg_counts.R)
791 available in **S1 File**.
792
793 **RNA-seq**. RNA was extracted from mock and infected samples at 24 hours post-infection
794 (MOI=0.05) using Qiagen RNeasy Kit. Samples were submitted for polyA-selected RNA (mRNA)
795 sequencing using an Illumina NovaSeq 6000 with 150 bp paired end reads at the University of
796 Illinois Urbana-Champaign Roy J. Carver Biotechnology Center. Reads were trimmed of adapter
797 sequences and low-quality reads eliminated using Trimmomatic (V0.32). Trimmed reads were
798 mapped to a hybrid reference genome (Gallus gallus GRCg7b, PR8, and $PR8_{CG}$) using STAR
799 (V2.7.11b) and quantified per feature using HTSeq (V2.0). Differential expression analysis was
800 performed using DESeq2 (v1.34.0). Data were processed and analyzed in R-Studio version
801 1.3.1073 using R language version 3.6.3. DESeq2 R code is available in **S2 File**. RNA-seq data
802 are available at the NCBI Sequence Read Archive (SRA) under accession code PRJNA1208514.
803
804 **Quantitative reverse-transcription PCR.** To quantify endogenous chicken *ZC3HAV1* and
805 *TUBA4A* mRNA transcripts in shRNA-expressing stable cells following chicken interferon-alpha
806 treatment (1000U/mL; Bio-Rad) for 24 hours, 500,000 cells were plated in 6-well plates and
807 allowed to adhere overnight in culture media followed by addition of chicken interferon or vehicle.
808 After 24 hours, cells were harvested, RNA extracted using Qiagen RNeasy kit, and cDNA
809 synthesized used Qiagen Quantitect Reverse Transcription Kit using supplied primer mix
810 (includes random hexamers and oligo-dT primers) with genomic DNA wipeout according to
811 manufacturer's instructions. To quantify *IAV segment 5 RNA* in mock and infected chicken DF-1
812 cells (input) and GFP-Trap immunoprecipitated (IP) samples, RNA extraction and cDNA synthesis
813 were performed as above. Quantitative PCR was performed in technical triplicate on a LightCycler
814 480 II (Roche Life Science) or QuantStudio5 (Applied Biosystems) using Ssofast Eva Green
815 Supermix (Bio-Rad). Oligonucleotide primer sequences are provided in **S1 Table**.
816
817 **Statistical analyses.** Plaque assay results from IAV infections were plotted in GraphPad Prism
818 10 and one-way ANOVA was used at 48 hours post-infection or two-way ANOVA for multiple time
819 points to determine statistical significance. Single-cycle ROSV and IAV infectivity results were
820 plotted in GraphPad Prism 10. Unpaired t tests were used to calculate statistical significance for

821 IAV single-cycle infectivity assays. Statistical analyses and graphed data values are available in
822 **S2 Table**.
823

824 **ACKNOWLEDGEMENTS**
825 We wish to thank members of both Langlois and Harris labs for helpful conversations. We wish
826 to acknowledge and thank Andrew Mehle for the A/green-wing teal/Ohio/1751986(H2N1)
827 OH175/S009 plasmids. This work was supported by NIAID grants R56-AI150965, R01-AI148669,
828 and NIH Centers for Excellence in Influenza Research and Response NHH75N93021C00017
829 awarded to RAL. Salary support for JTB was provided by NIAID F32-AI147813. RSH is an
830 Investigator of the Howard Hughes Medical Institute and the Ewing Halsell President's Council
831 Distinguished Chair. We thank the University of Illinois Roy J. Carver Biotechnology Center for
832 RNA and amplicon sequencing. RCAS GFP (CT#22) was a gift from Connie Cepko (Addgene
833 plasmid #13878). psPAX2 was a gift from Didier Trono (Addgene plasmid #12260). pMD2.G was
834 a gift from Didier Trono (Addgene plasmid #12259). pCAG RABV-G was a gift from Connie Cepko
835 (Addgene plasmid #36398). Polyclonal Anti-Influenza Virus, A/Puerto Rico/8/1934 (H1N1),
836 (antiserum, Rooster), NR-3098 was obtained through BEI Resources, NIAID, NIH. Monoclonal
837 Anti-Influenza A Virus Nucleoprotein (NP), Clone IC5-1B7 (produced in vitro), NR-43899 was
838 obtained through BEI Resources, NIAID, NIH. Anti-Human Immunodeficiency Virus 1 (HIV-1) p24
839 Hybridoma (183-H12-5C), ARP-1513, was obtained through the NIH HIV Reagent Program,
840 Division of AIDS, NIAID, NIH contributed by Dr. Bruce Chesebro and Dr. Hardy Chen. AMV-3C2
841 was deposited to the DSHB by Boettiger, D. (DSHB Hybridoma Product AMV-3C2).
842
843 **DECLARATION OF INTERESTS**
844 The authors have no competing interests to declare.
845

846 **REFERENCES**

847 1. Lai S, Qin Y, Cowling BJ, Ren X, Wardrop NA, Gilbert M, et al. Global epidemiology of avian
848 influenza A H5N1 virus infection in humans, 1997-2015: a systematic review of individual
849 case data. Lancet Infect Dis. 2016;16: e108–e118. doi:10.1016/S1473-3099(16)00153-5

850 2. Taubenberger JK, Morens DM. Influenza: the once and future pandemic. Public Health Rep
851 Wash DC 1974. 2010;125 Suppl 3: 16–26.

852 3. Taubenberger JK, Morens DM. 1918 Influenza: the mother of all pandemics. Emerg Infect
853 Dis. 2006;12: 15–22. doi:10.3201/eid1201.050979

854 4. Long JS, Mistry B, Haslam SM, Barclay WS. Host and viral determinants of influenza A virus
855 species specificity. Nat Rev Microbiol. 2019;17: 67–81. doi:10.1038/s41579-018-0115-z

856 5. Shi Y, Wu Y, Zhang W, Qi J, Gao GF. Enabling the “host jump”: structural determinants of
857 receptor-binding specificity in influenza A viruses. Nat Rev Microbiol. 2014;12: 822–831.
858 doi:10.1038/nrmicro3362

859 6. Walther T, Karamanska R, Chan RWY, Chan MCW, Jia N, Air G, et al. Glycomic analysis of
860 human respiratory tract tissues and correlation with influenza virus infection. PLoS Pathog.
861 2013;9: e1003223. doi:10.1371/journal.ppat.1003223

862 7. Galloway SE, Reed ML, Russell CJ, Steinhauer DA. Influenza HA subtypes demonstrate
863 divergent phenotypes for cleavage activation and pH of fusion: implications for host range
864 and adaptation. PLoS Pathog. 2013;9: e1003151. doi:10.1371/journal.ppat.1003151

865 8. Long JS, Giotis ES, Moncorgé O, Frise R, Mistry B, James J, et al. Species difference in
866 ANP32A underlies influenza A virus polymerase host restriction. Nature. 2016;529: 101–
867 104. doi:10.1038/nature16474

868 9. Van Valen L. A new evolutionary law. Evol Theory. 1973;1: 1–30.

869 10. Smyth RP, Negroni M, Lever AM, Mak J, Kenyon JC. RNA Structure-A Neglected Puppet
870 Master for the Evolution of Virus and Host Immunity. Front Immunol. 2018;9: 2097.
871 doi:10.3389/fimmu.2018.02097

872 11. Bermudez Y, Hatfield D, Muller M. A Balancing Act: The Viral-Host Battle over RNA Binding
873 Proteins. Viruses. 2024;16: 474. doi:10.3390/v16030474

874 12. Karlin S, Doerfler W, Cardon LR. Why is CpG suppressed in the genomes of virtually all
875 small eukaryotic viruses but not in those of large eukaryotic viruses? J Virol. 1994;68:
876 2889–2897. doi:10.1128/JVI.68.5.2889-2897.1994

877 13. Karlin S, Ladunga I, Blaisdell BE. Heterogeneity of genomes: measures and values. Proc
878 Natl Acad Sci U S A. 1994;91: 12837–12841. doi:10.1073/pnas.91.26.12837

879 14. Greenbaum BD, Levine AJ, Bhanot G, Rabadan R. Patterns of evolution and host gene
880 mimicry in influenza and other RNA viruses. PLoS Pathog. 2008;4: e1000079.
881 doi:10.1371/journal.ppat.1000079

882 15. Cooper DN, Gerber-Huber S. DNA methylation and CpG suppression. Cell Differ. 1985;17:
883 199–205. doi:10.1016/0045-6039(85)90488-9

884 16. Simmonds P, Xia W, Baillie JK, McKinnon K. Modelling mutational and selection pressures
885 on dinucleotides in eukaryotic phyla--selection against CpG and UpA in cytoplasmically
886 expressed RNA and in RNA viruses. BMC Genomics. 2013;14: 610. doi:10.1186/1471-
887 2164-14-610

888 17. Shaw AE, Rihn SJ, Mollentze N, Wickenhagen A, Stewart DG, Orton RJ, et al. The antiviral
889 state has shaped the CpG composition of the vertebrate interferome to avoid self-targeting.
890 PLoS Biol. 2021;19: e3001352. doi:10.1371/journal.pbio.3001352

891 18. Atkinson NJ, Witteveldt J, Evans DJ, Simmonds P. The influence of CpG and UpA
892 dinucleotide frequencies on RNA virus replication and characterization of the innate
893 cellular pathways underlying virus attenuation and enhanced replication. Nucleic Acids
894 Res. 2014;42: 4527–4545. doi:10.1093/nar/gku075

895 19. Gu H, Fan RLY, Wang D, Poon LLM. Dinucleotide evolutionary dynamics in influenza A
896 virus. Virus Evol. 2019;5: vez038. doi:10.1093/ve/vez038

897 20. Takata MA, Gonçalves-Carneiro D, Zang TM, Soll SJ, York A, Blanco-Melo D, et al. CG
898 dinucleotide suppression enables antiviral defence targeting non-self RNA. Nature. 2017.
899 doi:10.1038/nature24039

900 21. Ficarelli M, Wilson H, Pedro Galão R, Mazzon M, Antzin-Anduetza I, Marsh M, et al.
901 KHNYN is essential for the zinc finger antiviral protein (ZAP) to restrict HIV-1 containing
902 clustered CpG dinucleotides. eLife. 2019;8: e46767. doi:10.7554/eLife.46767

903 22. Li MMH, Aguilar EG, Michailidis E, Pabon J, Park P, Wu X, et al. Characterization of Novel
904 Splice Variants of Zinc Finger Antiviral Protein (ZAP). J Virol. 2019;93: e00715-19.
905 doi:10.1128/JVI.00715-19

906 23. Schwerk J, Soveg FW, Ryan AP, Thomas KR, Hatfield LD, Ozarkar S, et al. RNA-binding
907 protein isoforms ZAP-S and ZAP-L have distinct antiviral and immune resolution functions.
908 Nat Immunol. 2019;20: 1610–1620. doi:10.1038/s41590-019-0527-6

909 24. Kerns JA, Emerman M, Malik HS. Positive selection and increased antiviral activity
910 associated with the PARP-containing isoform of human zinc-finger antiviral protein. PLoS
911 Genet. 2008;4: e21. doi:10.1371/journal.pgen.0040021

912 25. Daugherty MD, Young JM, Kerns JA, Malik HS. Rapid evolution of PARP genes suggests a
913 broad role for ADP-ribosylation in host-virus conflicts. PLoS Genet. 2014;10: e1004403.
914 doi:10.1371/journal.pgen.1004403

915 26. Huang S, Girdner J, Nguyen LP, Sandoval C, Fregoso OI, Enard D, et al. Positive selection
916 analyses identify a single WWE domain residue that shapes ZAP into a more potent
917 restriction factor against alphaviruses. PLoS Pathog. 2024;20: e1011836.
918 doi:10.1371/journal.ppat.1011836

919 27. Zheng X, Wang X, Tu F, Wang Q, Fan Z, Gao G. TRIM25 Is Required for the Antiviral
920 Activity of Zinc Finger Antiviral Protein. J Virol. 2017;91: e00088-17.
921 doi:10.1128/JVI.00088-17

922 28. Li MMH, Lau Z, Cheung P, Aguilar EG, Schneider WM, Bozzacco L, et al. TRIM25
923 Enhances the Antiviral Action of Zinc-Finger Antiviral Protein (ZAP). PLoS Pathog.
924 2017;13: e1006145. doi:10.1371/journal.ppat.1006145

925 29. Kmiec D, Lista MJ, Ficarelli M, Swanson CM, Neil SJD. S-farnesylation is essential for
926 antiviral activity of the long ZAP isoform against RNA viruses with diverse replication
927 strategies. PLoS Pathog. 2021;17: e1009726. doi:10.1371/journal.ppat.1009726

928 30. Shaw AE, Hughes J, Gu Q, Behdenna A, Singer JB, Dennis T, et al. Fundamental
929 properties of the mammalian innate immune system revealed by multispecies comparison
930 of type I interferon responses. PLoS Biol. 2017;15: e2004086.
931 doi:10.1371/journal.pbio.2004086

932 31. Bouton CR, Domjanič GG, Lista MJ, Galão RP, Courty T, Wilson HD, et al. Defining the
933 ordered pathway for ZAP-mediated RNA decay. bioRxiv; 2025. p. 2025.04.28.650959.
934 doi:10.1101/2025.04.28.650959

935 32. Carlson CJ, Farrell MJ, Grange Z, Han BA, Mollentze N, Phelan AL, et al. The future of
936 zoonotic risk prediction. Philos Trans R Soc Lond B Biol Sci. 2021;376: 20200358.
937 doi:10.1098/rstb.2020.0358

938 33. Marco A, Marín I. CGIN1: a retroviral contribution to mammalian genomes. Mol Biol Evol.
939 2009;26: 2167–2170. doi:10.1093/molbev/msp127

940 34. Plianchaisuk A, Kusama K, Kato K, Sriswasdi S, Tamura K, Iwasaki W. Origination of LTR
941 Retroelement-Derived NYNRIN Coincides with Therian Placental Emergence. Mol Biol
942 Evol. 2022;39: msac176. doi:10.1093/molbev/msac176

943 35. Rabadan R, Levine AJ, Robins H. Comparison of avian and human influenza A viruses
944 reveals a mutational bias on the viral genomes. J Virol. 2006;80: 11887–11891.
945 doi:10.1128/JVI.01414-06

946 36. Zhang Y, Aevermann BD, Anderson TK, Burke DF, Dauphin G, Gu Z, et al. Influenza
947 Research Database: An integrated bioinformatics resource for influenza virus research.
948 Nucleic Acids Res. 2017;45: D466–D474. doi:10.1093/nar/gkw857

949 37. Pekarek MJ, Weaver EA. Existing Evidence for Influenza B Virus Adaptations to Drive
950 Replication in Humans as the Primary Host. Viruses. 2023;15: 2032.
951 doi:10.3390/v15102032

952 38. Sederdahl BK, Williams JV. Epidemiology and Clinical Characteristics of Influenza C Virus.
953 Viruses. 2020;12: 89. doi:10.3390/v12010089

954 39. Kistler KE, Bedford T. An atlas of continuous adaptive evolution in endemic human viruses.
955 Cell Host Microbe. 2023;31: 1898-1909.e3. doi:10.1016/j.chom.2023.09.012

956 40. Lowen AC. Constraints, Drivers, and Implications of Influenza A Virus Reassortment. Annu
957 Rev Virol. 2017;4: 105–121. doi:10.1146/annurev-virology-101416-041726

958 41. Karlberg T, Klepsch M, Thorsell A-G, Andersson CD, Linusson A, Schüler H. Structural
959 basis for lack of ADP-ribosyltransferase activity in poly(ADP-ribose) polymerase-13/zinc
960 finger antiviral protein. J Biol Chem. 2015;290: 7336–7344. doi:10.1074/jbc.M114.630160

961 42. Meagher JL, Takata M, Gonçalves-Carneiro D, Keane SC, Rebendenne A, Ong H, et al.
962 Structure of the zinc-finger antiviral protein in complex with RNA reveals a mechanism for
963 selective targeting of CG-rich viral sequences. Proc Natl Acad Sci U S A. 2019;116:
964 24303–24309. doi:10.1073/pnas.1913232116

965 43. Luo X, Wang X, Gao Y, Zhu J, Liu S, Gao G, et al. Molecular Mechanism of RNA
966 Recognition by Zinc-Finger Antiviral Protein. Cell Rep. 2020;30: 46-52.e4.
967 doi:10.1016/j.celrep.2019.11.116

968 44. Song Y, DiMaio F, Wang RY-R, Kim D, Miles C, Brunette T, et al. High-resolution
969 comparative modeling with RosettaCM. Struct Lond Engl 1993. 2013;21: 1735–1742.
970 doi:10.1016/j.str.2013.08.005

971 45. Baek M, DiMaio F, Anishchenko I, Dauparas J, Ovchinnikov S, Lee GR, et al. Accurate
972 prediction of protein structures and interactions using a three-track neural network.
973 Science. 2021;373: 871–876. doi:10.1126/science.abj8754

974 46. Varadi M, Anyango S, Deshpande M, Nair S, Natassia C, Yordanova G, et al. AlphaFold
975 Protein Structure Database: massively expanding the structural coverage of protein-
976 sequence space with high-accuracy models. Nucleic Acids Res. 2022;50: D439–D444.
977 doi:10.1093/nar/gkab1061

978 47. Gaunt E, Wise HM, Zhang H, Lee LN, Atkinson NJ, Nicol MQ, et al. Elevation of CpG
979 frequencies in influenza A genome attenuates pathogenicity but enhances host response
980 to infection. eLife. 2016;5: e12735. doi:10.7554/eLife.12735

981 48. Kimura M, Takatsuki A, Yamaguchi I. Blasticidin S deaminase gene from Aspergillus terreus
982 (BSD): a new drug resistance gene for transfection of mammalian cells. Biochim Biophys
983 Acta. 1994;1219: 653–659. doi:10.1016/0167-4781(94)90224-0

984 49. de Wispelaere M, Yang PL. Mutagenesis of the DI/DIII linker in dengue virus envelope
985 protein impairs viral particle assembly. J Virol. 2012;86: 7072–7083.
986 doi:10.1128/JVI.00224-12

987 50. Gonçalves-Carneiro D, Takata MA, Ong H, Shilton A, Bieniasz PD. Origin and evolution of
988 the zinc finger antiviral protein. PLoS Pathog. 2021;17: e1009545.
989 doi:10.1371/journal.ppat.1009545

990 51. Anantharaman V, Aravind L. The NYN domains: novel predicted RNAses with a PIN
991 domain-like fold. RNA Biol. 2006;3: 18–27. doi:10.4161/rna.3.1.2548

992 52. Youle RL, Lista MJ, Bouton C, Kunzelmann S, Wilson H, Cottee MA, et al. Structural and
993 functional characterization of the extended-diKH domain from the antiviral
994 endoribonuclease KHNYN. J Biol Chem. 2025;301: 108336. doi:10.1016/j.jbc.2025.108336

995 53. Yin Z, Kobayashi M, Hu W, Higashi K, Begum NA, Kurokawa K, et al. RNA-binding motifs of
996 hnRNP K are critical for induction of antibody diversification by activation-induced cytidine
997 deaminase. Proc Natl Acad Sci U S A. 2020;117: 11624–11635.
998 doi:10.1073/pnas.1921115117

999 54. Ficarelli M, Antzin-Anduetza I, Hugh-White R, Firth AE, Sertkaya H, Wilson H, et al. CpG
1000 Dinucleotides Inhibit HIV-1 Replication through Zinc Finger Antiviral Protein (ZAP)-
1001 Dependent and -Independent Mechanisms. J Virol. 2020;94: e01337-19.
1002 doi:10.1128/JVI.01337-19

1003 55. Galão RP, Wilson H, Schierhorn KL, Debeljak F, Bodmer BS, Goldhill D, et al. TRIM25 and
1004 ZAP target the Ebola virus ribonucleoprotein complex to mediate interferon-induced
1005 restriction. PLoS Pathog. 2022;18: e1010530. doi:10.1371/journal.ppat.1010530

1006 56. Müller S, Möller P, Bick MJ, Wurr S, Becker S, Günther S, et al. Inhibition of filovirus
1007 replication by the zinc finger antiviral protein. J Virol. 2007;81: 2391–2400.
1008 doi:10.1128/JVI.01601-06

1009 57. Fros JJ, Visser I, Tang B, Yan K, Nakayama E, Visser TM, et al. The dinucleotide
1010 composition of the Zika virus genome is shaped by conflicting evolutionary pressures in
1011 mammalian hosts and mosquito vectors. PLoS Biol. 2021;19: e3001201.
1012 doi:10.1371/journal.pbio.3001201

1013 58. Harris RS, Hultquist JF, Evans DT. The restriction factors of human immunodeficiency virus.
1014 J Biol Chem. 2012;287: 40875–40883. doi:10.1074/jbc.R112.416925

1015 59. Malim MH, Bieniasz PD. HIV Restriction Factors and Mechanisms of Evasion. Cold Spring
1016 Harb Perspect Med. 2012;2: a006940. doi:10.1101/cshperspect.a006940

1017 60. Yeoh ZC, Meagher JL, Kang C-Y, Bieniasz PD, Smith JL, Ohi MD. A minimal complex of
1018 KHNYN and zinc-finger antiviral protein binds and degrades single-stranded RNA. Proc
1019 Natl Acad Sci U S A. 2024;121: e2415048121. doi:10.1073/pnas.2415048121

1020 61. Odon V, Fiddaman SR, Smith AL, Simmonds P. Comparison of CpG- and UpA-mediated
1021 restriction of RNA virus replication in mammalian and avian cells and investigation of
1022 potential ZAP-mediated shaping of host transcriptome compositions. RNA N Y N. 2022;28:
1023 1089–1109. doi:10.1261/rna.079102.122

1024 62. Liu C-H, Zhou L, Chen G, Krug RM. Battle between influenza A virus and a newly identified
1025 antiviral activity of the PARP-containing ZAPL protein. Proc Natl Acad Sci U S A.
1026 2015;112: 14048–14053. doi:10.1073/pnas.1509745112

1027 63. Tang Q, Wang X, Gao G. The Short Form of the Zinc Finger Antiviral Protein Inhibits
1028 Influenza A Virus Protein Expression and Is Antagonized by the Virus-Encoded NS1. J
1029 Virol. 2017;91: e01909-16. doi:10.1128/JVI.01909-16

1030 64. Sharp CP, Thompson BH, Nash TJ, Diebold O, Pinto RM, Thorley L, et al. CpG dinucleotide
1031 enrichment in the influenza A virus genome as a live attenuated vaccine development
1032 strategy. PLoS Pathog. 2023;19: e1011357. doi:10.1371/journal.ppat.1011357

1033 65. Gorman OT, Bean WJ, Kawaoka Y, Webster RG. Evolution of the nucleoprotein gene of
1034 influenza A virus. J Virol. 1990;64: 1487–1497. doi:10.1128/JVI.64.4.1487-1497.1990

1035 66. Gammelin M, Altmüller A, Reinhardt U, Mandler J, Harley VR, Hudson PJ, et al.
1036 Phylogenetic analysis of nucleoproteins suggests that human influenza A viruses emerged
1037 from a 19th-century avian ancestor. Mol Biol Evol. 1990;7: 194–200.
1038 doi:10.1093/oxfordjournals.molbev.a040594

1039 67. Mehle A, Doudna JA. Adaptive strategies of the influenza virus polymerase for replication in
1040 humans. Proc Natl Acad Sci U S A. 2009;106: 21312–21316.
1041 doi:10.1073/pnas.0911915106

1042 68. Kosik I, Yewdell JW. Influenza Hemagglutinin and Neuraminidase: Yin¯Yang Proteins
1043 Coevolving to Thwart Immunity. Viruses. 2019;11: 346. doi:10.3390/v11040346

1044 69. Chen Y, Graf L, Chen T, Liao Q, Bai T, Petric PP, et al. Rare variant MX1 alleles increase
1045 human susceptibility to zoonotic H7N9 influenza virus. Science. 2021;373: 918–922.
1046 doi:10.1126/science.abg5953

1047 70. Mehle A, Dugan VG, Taubenberger JK, Doudna JA. Reassortment and mutation of the
1048 avian influenza virus polymerase PA subunit overcome species barriers. J Virol. 2012;86:
1049 1750–1757. doi:10.1128/JVI.06203-11

1050 71. Gonçalves-Carneiro D, Mastrocola E, Lei X, DaSilva J, Chan YF, Bieniasz PD. Rational
1051 attenuation of RNA viruses with zinc finger antiviral protein. Nat Microbiol. 2022;7: 1558–
1052 1567. doi:10.1038/s41564-022-01223-8

1053 72. Poulain F, Lejeune N, Willemart K, Gillet NA. Footprint of the host restriction factors
1054 APOBEC3 on the genome of human viruses. PLoS Pathog. 2020;16: e1008718.
1055 doi:10.1371/journal.ppat.1008718

1056 73. Moratorio G, Henningsson R, Barbezange C, Carrau L, Bordería AV, Blanc H, et al.
1057 Attenuation of RNA viruses by redirecting their evolution in sequence space. Nat Microbiol.
1058 2017;2: 17088. doi:10.1038/nmicrobiol.2017.88

1059 74. Simón D, Megrian D, Walt HK, Moreno P, Musto H, Hoffmann FG, et al. Impact of the Zinc
1060 Antiviral Protein on the genomic composition of RNA viruses infecting vertebrates. Mol Biol
1061 Evol. 2025; msaf135. doi:10.1093/molbev/msaf135

1062 75. Lo R, Gonçalves-Carneiro D. Sensing nucleotide composition in virus RNA. Biosci Rep.
1063 2023;43: BSR20230372. doi:10.1042/BSR20230372

1064 76. Judd EN, Gilchrist AR, Meyerson NR, Sawyer SL. Positive natural selection in
1065 primate genes of the type I interferon response. BMC Ecol Evol. 2021;21: 65.
1066 doi:10.1186/s12862-021-01783-z

1067 77. McDougal MB, Boys IN, De La Cruz-Rivera P, Schoggins JW. Evolution of the interferon
1068 response: lessons from ISGs of diverse mammals. Curr Opin Virol. 2022;53: 101202.
1069 doi:10.1016/j.coviro.2022.101202

1070 78. Daugherty MD, Malik HS. Rules of engagement: molecular insights from host-virus arms
1071 races. Annu Rev Genet. 2012;46: 677–700. doi:10.1146/annurev-genet-110711-155522

1072 79. Tenthorey JL, Emerman M, Malik HS. Evolutionary Landscapes of Host-Virus Arms Races.
1073 Annu Rev Immunol. 2022;40: 271–294. doi:10.1146/annurev-immunol-072621-084422

1074 80. Jones JE, Le Sage V, Padovani GH, Calderon M, Wright ES, Lakdawala SS. Parallel
1075 evolution between genomic segments of seasonal human influenza viruses reveals RNA-
1076 RNA relationships. eLife. 2021;10: e66525. doi:10.7554/eLife.66525

1077 81. Snoeck J, Fellay J, Bartha I, Douek DC, Telenti A. Mapping of positive selection sites in the
1078 HIV-1 genome in the context of RNA and protein structural constraints. Retrovirology.
1079 2011;8: 87. doi:10.1186/1742-4690-8-87

1080 82. Smith JD, McManus KF, Fraser HB. A novel test for selection on cis-regulatory elements
1081 reveals positive and negative selection acting on mammalian transcriptional enhancers.
1082 Mol Biol Evol. 2013;30: 2509–2518. doi:10.1093/molbev/mst134

1083 83. de Andrade KQ, Cirne-Santos CC. Antiviral Activity of Zinc Finger Antiviral Protein (ZAP) in
1084 Different Virus Families. Pathog Basel Switz. 2023;12: 1461.
1085 doi:10.3390/pathogens12121461

1086 84. Sharp CP, Thompson BH, Hoque AF, Diebold O, Tesla B, Kurian D, et al. Understanding
1087 off-target growth defects introduced to influenza A virus by synonymous recoding. RNA N
1088 Y N. 2025; rna.080675.125. doi:10.1261/rna.080675.125

1089 85. Goossens KE, Karpala AJ, Ward A, Bean AGD. Characterisation of chicken ZAP. Dev
1090 Comp Immunol. 2014;46: 373–381. doi:10.1016/j.dci.2014.05.011

1091 86. Gao G, Guo X, Goff SP. Inhibition of retroviral RNA production by ZAP, a CCCH-type zinc
1092 finger protein. Science. 2002;297: 1703–1706. doi:10.1126/science.1074276

1093 87. Becker JT, Sherer NM. Subcellular Localization of HIV-1 gag-pol mRNAs Regulates Sites of
1094 Virion Assembly. J Virol. 2017;91. doi:10.1128/JVI.02315-16

1095 88. Becker JT, Evans EL, Benner BE, Pritzl SL, Smith LE, Bates AE, et al. HIV-1 RNA genomes
1096 initiate host protein packaging in the cytosol independently of Gag capsid proteins. bioRxiv;
1097 2020. p. 846105. doi:10.1101/846105

1098 89. Iwatani Y, Chan DSB, Wang F, Stewart-Maynard K, Sugiura W, Gronenborn AM, et al.
1099 Deaminase-independent inhibition of HIV-1 reverse transcription by APOBEC3G. Nucleic
1100 Acids Res. 2007;35: 7096–7108. doi:10.1093/nar/gkm750

1101 90. Harris RS, Bishop KN, Sheehy AM, Craig HM, Petersen-Mahrt SK, Watt IN, et al. DNA
1102 deamination mediates innate immunity to retroviral infection. Cell. 2003;113: 803–809.

1103 91. Pollpeter D, Parsons M, Sobala AE, Coxhead S, Lang RD, Bruns AM, et al. Deep
1104 sequencing of HIV-1 reverse transcripts reveals the multifaceted antiviral functions of
1105 APOBEC3G. Nat Microbiol. 2018;3: 220–233. doi:10.1038/s41564-017-0063-9

1106 92. Moraes SN, Becker JT, Moghadasi SA, Shaban NM, Auerbach AA, Cheng AZ, et al.
1107 Evidence linking APOBEC3B genesis and evolution of innate immune antagonism by
1108 gamma-herpesvirus ribonucleotide reductases. eLife. 2022;11: e83893.
1109 doi:10.7554/eLife.83893

1110 93. Perreira JM, Chin CR, Feeley EM, Brass AL. IFITMs restrict the replication of multiple
1111 pathogenic viruses. J Mol Biol. 2013;425: 4937–4955. doi:10.1016/j.jmb.2013.09.024

1112 94. Ahi YS, Yimer D, Shi G, Majdoul S, Rahman K, Rein A, et al. IFITM3 Reduces Retroviral
1113 Envelope Abundance and Function and Is Counteracted by glycoGag. mBio. 2020;11:
1114 e03088-19. doi:10.1128/mBio.03088-19

1115 95. Johnson WE. Origins and evolutionary consequences of ancient endogenous retroviruses.
1116 Nat Rev Microbiol. 2019;17: 355–370. doi:10.1038/s41579-019-0189-2

1117 96. Lowen AC, Baker AL, Bowman AS, García-Sastre A, Hensley SE, Lakdawala SS, et al.
1118 Pandemic risk stemming from the bovine H5N1 outbreak: an account of the knowns and
1119 unknowns. J Virol. 2025;99: e0005225. doi:10.1128/jvi.00052-25

1120 97. Pasitka L, Cohen M, Ehrlich A, Gildor B, Reuveni E, Ayyash M, et al. Spontaneous
1121 immortalization of chicken fibroblasts generates stable, high-yield cell lines for serum-free
1122 production of cultured meat. Nat Food. 2023;4: 35–50. doi:10.1038/s43016-022-00658-w

1123 98. Dutko JA, Schäfer A, Kenny AE, Cullen BR, Curcio MJ. Inhibition of a yeast LTR
1124 retrotransposon by human APOBEC3 cytidine deaminases. Curr Biol CB. 2005;15: 661–
1125 666. doi:10.1016/j.cub.2005.02.051

1126 99. Krchlíková V, Fábryová H, Hron T, Young JM, Koslová A, Hejnar J, et al. Antiviral Activity
1127 and Adaptive Evolution of Avian Tetherins. J Virol. 2020;94: e00416-20.
1128 doi:10.1128/JVI.00416-20

1129 100. Becker JT, Auerbach AA, Harris RS. APEX3 - An Optimized Tool for Rapid and Unbiased
1130 Proximity Labeling. J Mol Biol. 2023;435: 168145. doi:10.1016/j.jmb.2023.168145

1131 101. Refsland EW, Stenglein MD, Shindo K, Albin JS, Brown WL, Harris RS. Quantitative
1132 profiling of the full APOBEC3 mRNA repertoire in lymphocytes and tissues: implications for
1133 HIV-1 restriction. Nucleic Acids Res. 2010;38: 4274–4284. doi:10.1093/nar/gkq174

1134 102. Quinlivan M, Zamarin D, García-Sastre A, Cullinane A, Chambers T, Palese P. Attenuation
1135 of equine influenza viruses through truncations of the NS1 protein. J Virol. 2005;79: 8431–
1136 8439. doi:10.1128/JVI.79.13.8431-8439.2005

1137 103. Gallois-Montbrun S, Kramer B, Swanson CM, Byers H, Lynham S, Ward M, et al. Antiviral
1138 protein APOBEC3G localizes to ribonucleoprotein complexes found in P bodies and stress
1139 granules. J Virol. 2007;81: 2165–2178. doi:10.1128/JVI.02287-06

1140 104. Evans EL, Becker JT, Fricke SL, Patel K, Sherer NM. HIV-1 Vif's Capacity To Manipulate
1141 the Cell Cycle Is Species Specific. J Virol. 2018;92. doi:10.1128/JVI.02102-17

1142 105. Chen CM, Smith DM, Peters MA, Samson ME, Zitz J, Tabin CJ, et al. Production and
1143 design of more effective avian replication-incompetent retroviral vectors. Dev Biol.
1144 1999;214: 370–384. doi:10.1006/dbio.1999.9432

1145 106. Li F, Sewald X, Jin J, Sherer NM, Mothes W. Murine leukemia virus Gag localizes to the
1146 uropod of migrating primary lymphocytes. J Virol. 2014;88: 10541–10555.
1147 doi:10.1128/JVI.01104-14

1148 107. Beier KT, Saunders A, Oldenburg IA, Miyamichi K, Akhtar N, Luo L, et al. Anterograde or
1149 retrograde transsynaptic labeling of CNS neurons with vesicular stomatitis virus vectors.
1150 Proc Natl Acad Sci U S A. 2011;108: 15414–15419. doi:10.1073/pnas.1110854108

1151 108. Carpenter MA, Law EK, Serebrenik A, Brown WL, Harris RS. A lentivirus-based system for
1152 Cas9/gRNA expression and subsequent removal by Cre-mediated recombination. Methods
1153 San Diego Calif. 2019;156: 79–84. doi:10.1016/j.ymeth.2018.12.006

1154 109. Park J, Bae S, Kim J-S. Cas-Designer: a web-based tool for choice of CRISPR-Cas9
1155 target sites. Bioinforma Oxf Engl. 2015;31: 4014–4016. doi:10.1093/bioinformatics/btv537

1156 110. Sanjana NE, Shalem O, Zhang F. Improved vectors and genome-wide libraries for
1157 CRISPR screening. Nat Methods. 2014;11: 783–784. doi:10.1038/nmeth.3047

1158 111. Moffat J, Grueneberg DA, Yang X, Kim SY, Kloepfer AM, Hinkle G, et al. A lentiviral RNAi
1159 library for human and mouse genes applied to an arrayed viral high-content screen. Cell.
1160 2006;124: 1283–1298. doi:10.1016/j.cell.2006.01.040

1161 112. Ory DS, Neugeboren BA, Mulligan RC. A stable human-derived packaging cell line for
1162 production of high titer retrovirus/vesicular stomatitis virus G pseudotypes. Proc Natl Acad
1163 Sci U S A. 1996;93: 11400–11406. doi:10.1073/pnas.93.21.11400

1164 113. Naldini L, Blömer U, Gallay P, Ory D, Mulligan R, Gage FH, et al. In vivo gene delivery and
1165 stable transduction of nondividing cells by a lentiviral vector. Science. 1996;272: 263–267.
1166 doi:10.1126/science.272.5259.263

1167 114. Wang J, Becker JT, Shi K, Lauer KV, Salamango DJ, Aihara H, et al. The Role of RNA in
1168 HIV-1 Vif-Mediated Degradation of APOBEC3H. J Mol Biol. 2019;431: 5019–5031.
1169 doi:10.1016/j.jmb.2019.09.014

1170 115. Brinkman EK, Chen T, Amendola M, van Steensel B. Easy quantitative assessment of
1171 genome editing by sequence trace decomposition. Nucleic Acids Res. 2014;42: e168.
1172 doi:10.1093/nar/gku936

1173 116. Sjaastad LE, Fay EJ, Fiege JK, Macchietto MG, Stone IA, Markman MW, et al. Distinct
1174 antiviral signatures revealed by the magnitude and round of influenza virus replication in
1175 vivo. Proc Natl Acad Sci U S A. 2018;115: 9610–9615. doi:10.1073/pnas.1807516115

1176 117. Waring BM, Sjaastad LE, Fiege JK, Fay EJ, Reyes I, Moriarity B, et al. MicroRNA-Based
1177 Attenuation of Influenza Virus across Susceptible Hosts. J Virol. 2018;92.
1178 doi:10.1128/JVI.01741-17

1179 118. Phan T, Ye Q, Stach C, Lin Y-C, Cao H, Bowen A, et al. Synthetic Cell Lines for Inducible
1180 Packaging of Influenza A Virus. ACS Synth Biol. 2024;13: 546–557.
1181 doi:10.1021/acssynbio.3c00526

1182

1183 **FIGURE LEGENDS**

1184

1185 **Fig 1. Chicken and duck ZAP do not potently restrict replication of PR8 IAV or CpG-**
1186 **enriched PR8 IAV.**

1187 **(A)** IAV sequences exhibit depletion of CpG content (CpG per kb = # CpG / segment length in
1188 kilobases [kb]). Box and whisker plots showing CpG content of all IAV sequences from avian
1189 (orange), human (blue), and swine (green) hosts as well as IBV (pink) and ICV (purple). Thick
1190 black bars represent median CpG content, boxes define the 25th to 75th percentile, and whiskers
1191 represent range excluding outliers. Horizontal dashed gray lines highlight median avian IAV CpG
1192 content as a reference.

1193 **(B)** Schematic of human ZAP-L, human ZAP-S and chicken ZAP (ggaZAP) protein domain
1194 architecture including four CCCH zinc fingers and inactive poly-ADP ribose polymerase (iPARP).
1195 Amino acid alignment of ZAP zinc finger 2 (ZF2; human residues 88-110) from multiple species.
1196 Conserved CCCH residues are highlighted with green vertical bars.

1197 **(C)** CpG content of PR8 (shades of gray by segment length), wild-type NP (blue), and CpG-
1198 enriched NP (orange) calculated as # CpG per 100 nucleotides (nt) over a sliding window (top).
1199 Schematic of PR8 and $PR8_{CG}$ viruses and displaying CpG content for each virus and total CpG
1200 number encoded by each NP segment (bottom).

1201 **(D)** Titers of PR8 and $PR8_{CG}$ at 48 hours post infection (hpi) in chicken DF-1 cells stably
1202 expressing mNeonGreen (mNG, gray), mNG-tagged chicken ZAP (mNG-ggaZAP, yellow), or
1203 untagged ggaZAP (orange) as well as control transduced cells (Vector, black). Bar represents
1204 mean plaque forming units per mL (PFU/mL) with error bars representing standard deviation of
1205 the mean. Multiplicity of infection (MOI) = 0.05 (pfu per cell).

1206 **(E)** Fluorescence images of DF-1 cells expressing mNG as well as fusion proteins of mNG-
1207 ggaZAP and mutants indicated (green, top). Nuclei counterstained with DAPI (blue) and shown
1208 in merge image (bottom). Scale bars represent 10 microns.

1209 **(F)** Titers of PR8 and $PR8_{CG}$ over 48 hpi in chicken DF-1 cells stably expressing mNG (black
1210 circles), mNG-ggaZAP (orange circles), mNG-hZF2 (green circles), mNG-C710S (orange/gray
1211 squares), and mNG-hZF2.C710S (green/gray diamonds) mutants shown in **(E)**. MOI=0.05.

1212 **(G)** Titers of PR8 and $PR8_{CG}$ at 48 hpi in parental untransduced DF-1 cells (DF-1, black), pooled
1213 CRISPR/Cas9 knockout chicken DF-1 cells expressing a control sgRNA targeting E. coli LacZ
1214 (LacZ, gray), or sgRNAs targeting endogenous chicken ZC3HAV1 (ggaZAP1-3 KO, shades of
1215 orange). MOI=0.05.

1216 **(H)** Titers of PR8 and $PR8_{CG}$ at 48 hpi in parental untransduced CCL-141 cells (CCL-141, black),
1217 pooled CRISPR/Cas9 knockout duck CCL-141 cells expressing a control sgRNA targeting E. coli
1218 LacZ (LacZ, gray), or sgRNAs targeting endogenous duck ZC3HAV1 (aplZAP1-3 KO, shades of
1219 yellow). MOI=0.05.
1220
1221 **Fig 2. Human ZAP-S and KHNYN can independently restrict CpG-enriched PR8 IAV.**
1222 **(A)** Titers of PR8 and $PR8_{CG}$ over 48 hpi in chicken DF-1 cells stably expressing human ZAP-L
1223 (orange circles), ZAP-S (green circles), KHNYN (blue circles), dKHNYN (gray circles), or TRIM25
1224 (pink circles) relative to Vector (black circles). MOI=0.05. *** indicates $p \leq 0.0001$ at 48hpi by two-
1225 way ANOVA.
1226 **(B)** Titers of PR8 and $PR8_{CG}$ over 48 hpi in chicken DF-1 cells stably expressing RNA-binding
1227 mutants of ZAP-S (green circles) including Y108A (green squares, dashed line) and chimeric
1228 encoding chicken ZF2 (gZF2; gray diamonds, dashed line) relative to Vector (black circles).
1229 MOI=0.05. ** indicates p=0.0093 at 48hpi by two-way ANOVA.
1230 **(C)** Titers of PR8 and $PR8_{CG}$ over 48 hpi in chicken DF-1 cells stably expressing C-terminal
1231 mutants of human ZAP-L (orange circles) and ZAP-S (green circles) including ZAP-L C899S
1232 (oranges squares, dashed line) and ZAP-S +CVIS motif (CVIS; green diamonds, dashed line).
1233 MOI=0.05. * indicates p=0.0108 at 48hpi by two-way ANOVA.
1234 **(D)** Titers of PR8 and $PR8_{CG}$ over 48 hpi in chicken DF-1 cells stably expressing mutants of
1235 KHNYN (blue circles) including catalytically inactive dKHNYN (gray circles), $_{95}$AQ/DE$_{96}$ mutant
1236 (AQDE; blue squares, dashed line), and combination mutant of dKHNYN with AQDE (dAQDE;
1237 gray diamond, dashed line). MOI=0.05. * indicates p=0.0158 at 48hpi by two-way ANOVA.
1238 **(E-H)** Western blots of chicken DF-1 cells stably expressing human ZAP, KHNYN, or TRIM25 and
1239 mutants used in **(A-D)** detecting ZAP, KHNYN, and/or TRIM25 as well as tubulin (TUBA) or
1240 histone 3 (H3) loading controls.
1241
1242 **Fig 3. Endogenous human ZAP and KHNYN can independently restrict CpG-enriched PR8**
1243 **IAV.**
1244 **(A)** Schematic depicting exon organization of human ZAP (green), KHNYN (blue), and TRIM25
1245 (pink) genes and sites targeted by CRISPR single guide RNAs (sgRNAs; carets). Colored boxes
1246 indicate coding exons and white boxes indicate noncoding portions of exons.
1247 **(B)** Western blots of CRISPR/Cas9 engineered knockout (KO) human A549 cell lines including
1248 parental A549 cells, control clone transduced with pLentiCRISPR1000 (Vector), control clone
1249 targeting E. coli LacZ (LacZ), two ZAP KO clones (ZAP1 and ZAP2), two KHNYN KO clones (K1

1250 and K2), two ZAP and KHNYN dual KO clones (ZK1 and ZK2), and two TRIM25 KO clones (T1
1251 and T2). Cells were treated with vehicle (PBS) or 1000 units per mL (U/mL) universal interferon-
1252 alpha (IFNα) for 24 hours. Histone H3 detected as loading control.
1253 **(C)** Titers of PR8 and $PR8_{CG}$ at 48 hpi in human A549 KO cells including parental (black), Vector
1254 and LacZ (shades of gray), ZAP KO clones (shades of green), and KHNYN KO clones (shades
1255 of blue). MOI=0.05.
1256 **(D)** Titers of PR8 and $PR8_{CG}$ at 48 hpi in human A549 KO cells including parental (black), Vector
1257 (gray), and ZAP+KHNYN KO clones (green and blue striped). MOI=0.05. *** indicates $p \leq 0.0001$
1258 and ** indicates p=0.0045 by one-way ANOVA.
1259 **(E)** Titers of PR8 and $PR8_{CG}$ at 48 hpi in human A549 KO cells including parental (black), LacZ
1260 (gray), and TRIM25 KO clones (shades of pink). MOI=0.05.
1261
1262 **Figure 4 Prenylated human ZAP and mammalian KHNYN can independently restrict**
1263 **naturally CpG-enriched ROSV.**
1264 **(A)** CpG content of retroviruses (ROSV in black, ROSV-mCherry reporter virus in pink dashed
1265 line, MLV in orange, and HIV-1 in blue) calculated as # CpG per 100 nucleotides over a sliding
1266 window (graph). Schematic of retrovirus open reading frame (ORF) organization (top).
1267 **(B)** Schematic of retroviral assembly and single-cycle infectivity assay including plasmid
1268 transfection into cells, cell lysate and supernatant harvest at 48 hours post-transfection (hpt),
1269 storage, and western blotting as well as DT40 suspension cell infection and flow cytometry as a
1270 measure of infectivity.
1271 **(C)** Retroviral assembly and single-cycle infectivity results of human ZAP-L, ZAP-S, and mutants
1272 effects on ROSV showing relative percent ROSV infected cells (% mCherry positive; % mCh+)
1273 as determined by flow cytometry. DF-1 cells transfected with increasing plasmid amounts of
1274 indicated host proteins (100, 200, or 400ng), 1500ng ROSV, and 200ng VSV-G. Infectivity is
1275 relative to backbone pcDNA3.2 transfections (Mock). Below, western blots detecting ROSV
1276 cleaved Gag^{p19} in supernatant virions as well as full-length ROSV Gag^{Pr76}, ZAP proteins, and
1277 ACTIN loading controls from cellular lysates.
1278 **(D)** Retroviral assembly and single-cycle infectivity results of human ZAP-L, chicken (gga) ZAP,
1279 duck (apl) ZAP, and prenylation mutant on ROSV infectivity. Below, western blots detecting ROSV
1280 cleaved Gag^{p19} in supernatant virions as well as full-length ROSV Gag^{Pr76}, mNG-tagged ZAP
1281 proteins, and ACTIN loading controls from cellular lysates.
1282 **(E)** Retroviral assembly and single-cycle infectivity results of human KHNYN, mutants, and
1283 mammalian KHNYN homologues (from pig, dog, and platypus) on ROSV infectivity. Below,

1284 western blots detecting ROSV cleaved Gag^{p19} in supernatant virions as well as full-length ROSV
1285 Gag^{Pr76}, human KHNYN proteins, and ACTIN loading controls from cellular lysates. Note
1286 mammalian KHNYN orthologues were not detected by human KHNYN antibodies.
1287 **(F)** Single-cycle infectivity (%mCh+ or %NP+) in A549 stable cells expressing YFP alone (black)
1288 and YFP-tagged platypus KHNYN (blue) effects on single-cycle IAV including laboratory PR8,
1289 pandemic Cal04, and avian-origin OH175. *** indicates p=0.000832, * indicates p=0.025875, and
1290 ** indicates p=0.002263 by unpaired t test.
1291 **(G)** IAV Minigenome reporter assay comparing mNG-tagged mammalian KHNYN (shades of blue:
1292 human, pig, dog, and platypus) relative to mNG alone (black) effects on IAV vRNA production (%
1293 mCh+ cells) using PB2, PB1, PA, and NP expression plasmids and a negative-sense mCherry
1294 vRNA reporter plasmid (encoding 34 CpG dinucleotides within the proxy vRNA).
1295

1296 **SUPPLEMENTAL FIGURE LEGENDS**

1297

1298 **S1 Fig. Mammalian IAV sequences are CpG-depleted over time relative to avian IAV.**

1299 **(A)** IAV sequences from human (blue) and swine (green) hosts exhibit depletion of CpG content
1300 (CpG per kb = # CpG / segment length in kilobases (kb)) relative to avian (orange) IAV over time
1301 since 1918. IBV (pink) and ICV (purple) exhibit relatively stable but dramatically lower CpG
1302 content than all IAV segments. Thick lines represent linear trend of data surrounded by 95%
1303 confidence interval in lighter shading.

1304 **(B)** CpG content of IAV sequences from avian, human, and swine segregated by virus segment.
1305 Segments 1-3 include PB2, PB1, and PA encoding the viral Polymerase. Segments 4-6 include
1306 HA, NP, and NA encoding virion proteins often subject to adaptive immune pressure. Segments
1307 7-8 include M and NS.

1308 **(C)** CpG content of IAV sequences from avian, human, and swine hosts segregated by common
1309 HA and NA subtypes.

1310 **(D)** CpG content of IAV sequences segregated by time periods indicated on the x-axis (top).
1311 Schematic of IAV natural history showing avian H1N1, H2N1, and H3N2 in orange shaded lines,
1312 human circulating subtypes in shaded blue lines, 2009 H1N1 pandemic swine flu in green lines,
1313 (middle) and source of reassortant segments in matched colors (bottom).

1314 Thick black bars represent median CpG content, boxes define the 25th to 75th percentile, and
1315 whiskers represent range excluding outliers. Horizontal dashed gray lines highlight median avian
1316 IAV CpG content as a reference.

1317

1318 **S2 Fig. Dinucleotide content of influenza viruses.**

1319 **(A)** CpG content as the normalized rho (ρ = #CpG / length divided by the product of #C / length
1320 and #G per length) of all IAV sequences from avian, human, and swine hosts as well as IBV and
1321 ICV.

1322 **(B)** Percent GC content (%GC = (#G + #C) / total length) all IAV sequences from avian, human,
1323 and swine hosts as well as IBV and ICV.

1324 **(C)** GpC content of all IAV sequences from avian, human, and swine hosts as well as IBV and
1325 ICV.

1326 **(D)** Remaining dinucleotide content of all IAV sequences from avian, human, and swine hosts as
1327 well as IBV and ICV.

1328

1329 **S3 Fig. Structural comparison of avian ZAP proteins and data for avian ZAP expression**
1330 **and knockdowns.**
1331 **(A)** Structure and model of human (blue; PDB: 6UEJ), chicken (RobettaCM, orange), chicken
1332 (RoseTTAFold, medium orange), and chicken (AlphaFold2, light orange) ZAP zinc fingers (1-4)
1333 with a CpGpU RNA oligonucleotide (gray; PDB: 6UEJ).
1334 Structure and model of human (blue; PDB: 6UEJ), duck (RobettaCM, green), duck
1335 (RoseTTAFold, medium green), and duck (AlphaFold2, light green) ZAP zinc fingers (1-4) with a
1336 CpGpU RNA oligonucleotide (gray; PDB: 6UEJ).
1337 Structure and model of human (blue; PDB: 6UEJ), quail (RobettaCM, pink), quail (RoseTTAFold,
1338 medium pink), and quail (AlphaFold2, light pink) ZAP zinc fingers (1-4) with a CpGpU RNA
1339 oligonucleotide (gray; PDB: 6UEJ).
1340 Structure and model of human (blue; PDB: 6UEJ), chicken (RobettaCM, orange), duck
1341 (RobettaCM, green), and chicken (AlphaFold2, light pink) ZAP zinc fingers (1-4) with a CpGpU
1342 RNA oligonucleotide (gray; PDB: 6UEJ).
1343 **(B)** Root mean squared deviation (RMSD) of structures and models in (A-D).
1344 **(C)** Western blots of chicken DF-1 cells stably expressing mNG, mNG-ggaZAP, and untagged
1345 ggaZAP as well as Vector transduced cells detecting mNG and blasticidin S deaminase (BSD).
1346 Actin detected as a loading control.
1347 **(D)** Western blots of chicken DF-1 cells stably expressing mNG, mNG-ggaZAP, and mutants of
1348 mNG-ggaZAP as well as Vector transduced cells detecting mNG and BSD. Actin detected as a
1349 loading control.
1350 **(E)** qPCR results detecting endogenous gga *ZC3HAV1* mRNA in chicken DF-1 cells transduced
1351 with lentiviruses expressing shRNAs indicated (shades of gray) following treatment with 1000
1352 U/mL of chicken interferon-alpha (IFN) relative to mock treated cells normalized to gga *TUBA1A*
1353 using a 2^{-ddCt} calculation.
1354 **(F)** Titers of PR8 and $PR8_{CG}$ over 48 hpi in chicken DF-1 cells stably expressing shRNAs targeting
1355 endogenous ggaZAP (shggaZAP1-3, shades of gray triangles/diamonds/hexagons), a control
1356 scrambled sequence siRNA (shScramble, dark gray squares), and parental untransduced DF-1
1357 cells (black circles). MOI=0.05.
1358 **(G)** Titers of PR8 and $PR8_{CG}$ at 48 hpi in duck CCL-141 cells transiently transfected with 1nM or
1359 10nM siRNAs targeting endogenous aplZAP (siZAP, shades of yellow), a control scrambled
1360 sequence siRNA (siNeg, 5nM, gray), and parental untransfected (black) CCL-141 cells.
1361 MOI=0.05.

1362 **(H)** Western blots of chicken DF-1 cells stably expressing human ZAP-L, ZAP-S, KHNYN, and
1363 TRIM25 as well as dually transduced ZAP-L or ZAP-S with KHNYN or dKHNYN including Vector
1364 transduced cells detecting ZAP and KHNYN. GAPDH detected as a loading control.
1365
1366 **S4 Fig. TIDE analysis of pooled CRISPR/Cas9 chicken DF-1 and duck CCL-141**
1367 **ZC3HAV1/ZAP knockouts.**
1368 **(A-B)** Schematic depicting exon organization of chicken ZC3HAV1/ZAP (orange) and duck
1369 ZC3HAV1/ZAP (yellow) as well as sites targeted by CRISPR single guide RNAs (sgRNAs;
1370 scissors). Colored boxes indicate coding exons and white boxes indicate noncoding portions of
1371 exons. Genomic sequence targeted by sgRNAs (underlined) and protospacer adjacent motif
1372 (PAM, lowercase) and amino acids encoding by that region (bold residues overlap sgRNA target).
1373 Genomic distances are relative and total locus size indicated.
1374 **(C)** Total knockout efficiency as determined by tracking of indels by decomposition (TIDE)
1375 analysis (% Knockout) in each pool relative to LacZ control cells.
1376 **(D-F)** TIDE analysis showing percent of sequences in pool exhibiting indicated indel (-10 to +10
1377 bp from expected cut site) in chicken ZC3HAV1-targeted KO DF-1 cells.
1378 **(G-I)** TIDE analysis showing percent of sequences in pool exhibiting indicated indel (-10 to +10
1379 bp from expected cut site) in duck ZC3HAV1-targeted KO CCL-141 cells.
1380 Red bars indicate disruptive indels (CRISPR-mediated insertions or deletions resulting in out-of-
1381 frame mutations). Gray bars indicate un-edited sequences. Black bars indicate in-frame indels
1382 (CRISPR-mediated insertions or deletions resulting in amino acid deletions).
1383
1384 **S5 Fig. Genetic and genomic comparisons of KHNYN genes**
1385 **(A)** Synteny diagrams of KHNYN genomic organization in representative species. KHNYN gene
1386 in blue, NYNRIN in magenta, neighboring human/pig/koala genes in black, neighboring platypus
1387 genes in red, and human/chicken genes syntenic to red genes in gray. Distances are relative and
1388 approximate size of locus shown on the right in kilobasepairs (Kbp).
1389 **(B)** Schematic of exon organization (left) and protein domain architecture (right) of human N4BP1
1390 (pink), KHNYN (blue), and NYNRIN (magenta). KH domain represents the extended HNRNPK-
1391 like, GXXG-like motif residues typical of KH-domains are indicated, NYN represents the NYN/PIN
1392 endonuclease domain, and CU represents cullin-binding domain associated with NEDD8
1393 (KHNYN and NYNRIN) or cousin of CUBAN domain (N4BP1).
1394 **(C)** Maximum likelihood phylogeny of all ensembl-annotated orthologues of human KHNYN,
1395 NYNRIN, and N4BP1.

1396 **(D)** Synteny diagrams and schematics of exon organization for alligator, anole, and zebrafish
1397 *"khnyn-like"* genes.
1398 **(E)** Structural predictions in three views of human (dark blue), pig (medium blue), dog (cyan), and
1399 platypus (lime green) KHNYN (residues 1-213). Putative GXXG motif highlighted by dashed black
1400 circle. Platypus-specific short loop highlighted by dashed black square.
1401
1402 **S6 Fig. YFP-tagged human ZAP-S and KHNYN inhibit $PR8_{CG}$ and OH175 IAV.**
1403 **(A)** Titers of PR8, $PR8_{CG}$. and avian OH175 at 48 hpi in chicken DF-1 cells stably expressing
1404 YFP-tagged human ZAP-L (orange), human ZAP-S (green), chicken ggaZAP (orange/gray),
1405 KHNYN (blue), dKHNYN (gray) and platypus oanKHNYN (pale blue) relative to YFP alone (black).
1406 MOI=0.05.
1407 **(B)** Western blots of chicken DF-1 cells used in (A) detecting YFP. Histone H3 detected as a
1408 loading control.
1409 **(C)** CpG content of OH175 (shades of red by segment length), OH175 segment 3 PA bolded line,
1410 as well as PR8 segment 3 PA (bold blue line) calculated as # CpG per 100 nucleotides (nt) over
1411 a sliding window (top). Schematic of PR8 and OH175 viruses and displaying CpG content for
1412 each virus and total CpG number encoded by each PA segment (bottom).
1413 **(D)** Fold enrichment by qPCR for PR8 IAV segment 5 NP RNA following GFP-Trap
1414 immunoprecipitation of indicated YFP-tagged proteins from chicken DF-1 cells uninfected or
1415 infected with PR8 or $PR8_{CG}$. MOI=5. Fold enrichment is shown relative to parental chicken DF-1
1416 cells lacking YFP, similar to an IgG isotype control used in chromatin immunoprecipitation (ChIP-
1417 qPCR) using a 2^{-ddCt} calculation. Western blots detecting YFP in IP (top) and YFP and IAV NP in
1418 Input (bottom). Actin detected as loading control.
1419
1420 **S7 Fig. Chicken and IAV transcriptome largely unaffected by human ZAP or KHNYN.**
1421 **(A)** Principal component analysis (PCA) of RNA-seq data.
1422 **(B)** Heatmap showing differentially expressed IAV mRNAs.
1423 **(C)** Heatmap showing most differentially expressed chicken mRNAs.
1424
1425 **S8 Fig. Platypus KHNYN is a potent and broadly acting antiviral protein.**
1426 **(A)** Retroviral assembly and single-cycle infectivity results of mammalian ZAP-L and ZAP-S
1427 homologues including pig, dog, and platypus on ROSV infectivity (relative infectivity, %mCh+).
1428 Platypus encodes a well annotated ZAP-L homologue but not a ZAP-S, a C653S prenylation
1429 mutant was included.

1430 **(B)** Retroviral assembly and single-cycle infectivity results of mammalian KHNYN homologues
1431 including pig, dog, and platypus as well as catalytically inactivated (*"d"*) mutants of each on ROSV
1432 infectivity.
1433 **(C)** Retroviral assembly and single-cycle infectivity results of platypus KHNYN including truncation
1434 mutants on ROSV infectivity (top). Schematic of protein domain architecture of platypus KHNYN
1435 with arrows indicating position of truncating stop mutation (bottom).
1436 **(D)** Retroviral assembly and single-cycle infectivity results of platypus KHNYN including truncation
1437 mutants on ROSV infectivity (top). Indication (bottom) of virus tested (HIV-mCh, HIV_{CG}-mCh, or
1438 MLV-mCh) and glycoprotein used for pseudotyping (HIV-1 Env, VSV-G, or RABV-G).
1439 **(E)** Retroviral assembly and single-cycle infectivity results of mammalian KHNYN homologues
1440 including pig, dog, and platypus as well as catalytically inactivated (*"d"*) mutants of each on ROSV
1441 infectivity in chicken ZAP knockout DF-1 cells (ggaZAP-3 KO from **Fig 1G, S4C Fig, and S4F**
1442 **Fig**).
1443
1444 **S9 Fig. ZAP localization conferred by prenylation motif in mammal and avian species.**
1445 **(A)** Fluorescence images of DF-1 cells expressing mNG as well as fusion proteins of mNG-ZAP
1446 orthologues and mutants indicated (green). Cell and nuclei outline in dashed white lines. Scale
1447 bars represent 10 microns.
1448 **(B)** Amino acid alignment of CaaX prenylation motif from multiple species indicated.
1449
1450 **S10 Fig. Conservation of mammalian KHNYN endonuclease domain and mammalian**
1451 **KHNYN subcellular localization.**
1452 **(A)** Amino acid alignment of NYN/PIN endonuclease domain (human residues 437-589) from
1453 multiple species KHNYN orthologues indicated.
1454 **(B)** Structural predictions in three views of human (dark blue), pig (medium blue), dog (cyan), and
1455 platypus (lime green) KHNYN (residues 437-589). Catalytic aspartic acid residues highlighted by
1456 dashed black circle.
1457 **(C)** Fluorescence images of DF-1 cells expressing mNG as well as fusion proteins of mNG-
1458 KHNYN orthologues and mutants indicated (green). Cell and nuclei outline in dashed white lines.
1459 Scale bars represent 10 microns.
1460
1461 **S1 Table. Key reagents.** Spreadsheet
1462 **S2 Table. Statistical analyses and graphed values.** Spreadsheet
1463

S1 File. Influenza sequences analysis R code. Text files

S2 File. DEseq2 analysis R code. Text files

S1 Data. Human and avian ZAP structural models. Python files open in UCSC Chimera

S2 Data. Mammalian KHNYN structural models of KH region. Python files open in UCSC Chimera

S3 Data. Mammalian KHNYN structural models of NYN domain. Python files open in UCSC Chimera

S4 Data. N4BP1, KHNYN, and NYNRIN phylogenetic data. Clustal nucleotide alignment, pdf of phylogenetic tree

S5 Data. ZC3HAV1/ZAP phylogenetic data. Clustal nucleotide alignment, pdf of phylogenetic tree

Figure 1

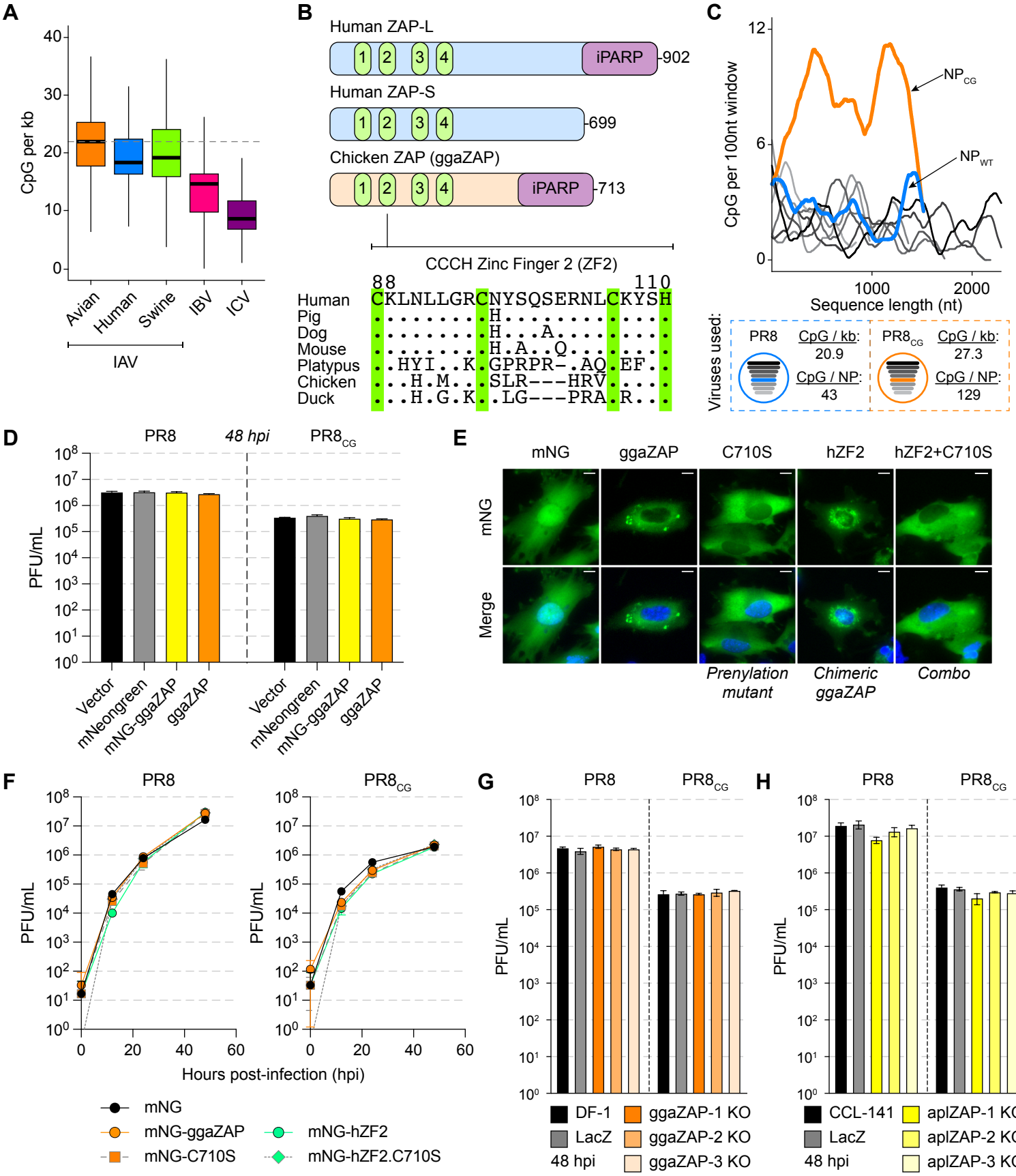
A
CpG per kb
Avian
Human
Swine
IBV
ICV
IAV
B
Human ZAP-L
iPARP
902
Human ZAP-S
699
Chicken ZAP (ggaZAP)
713
CCCH Zinc Finger 2 (ZF2)
88
110
Human CKLNLLGRCNYSQSERNLCKYSH
Pig
Dog
Mouse
Platypus
Chicken
Duck
C
CpG per 100nt window
NP_CG
NP_WT
Sequence length (nt)
Viruses used:
PR8
CpG / kb: 20.9
CpG / NP: 43
PR8_CG
CpG / kb: 27.3
CpG / NP: 129
D
PR8
48 hpi
PR8_CG
PFU/mL
Vector
mNeongreen
mNG-ggaZAP
ggaZAP
E
mNG
ggaZAP
C710S
hZF2
hZF2+C710S
Merge
Prenylation mutant
Chimeric ggaZAP
Combo
F
PR8
PR8_CG
PFU/mL
Hours post-infection (hpi)
mNG
mNG-ggaZAP
mNG-C710S
mNG-hZF2
mNG-hZF2.C710S
G
PR8
PR8_CG
DF-1
LacZ
48 hpi
ggaZAP-1 KO
ggaZAP-2 KO
ggaZAP-3 KO
H
PR8
PR8_CG
CCL-141
LacZ
48 hpi
aplZAP-1 KO
aplZAP-2 KO
aplZAP-3 KO

Figure 2

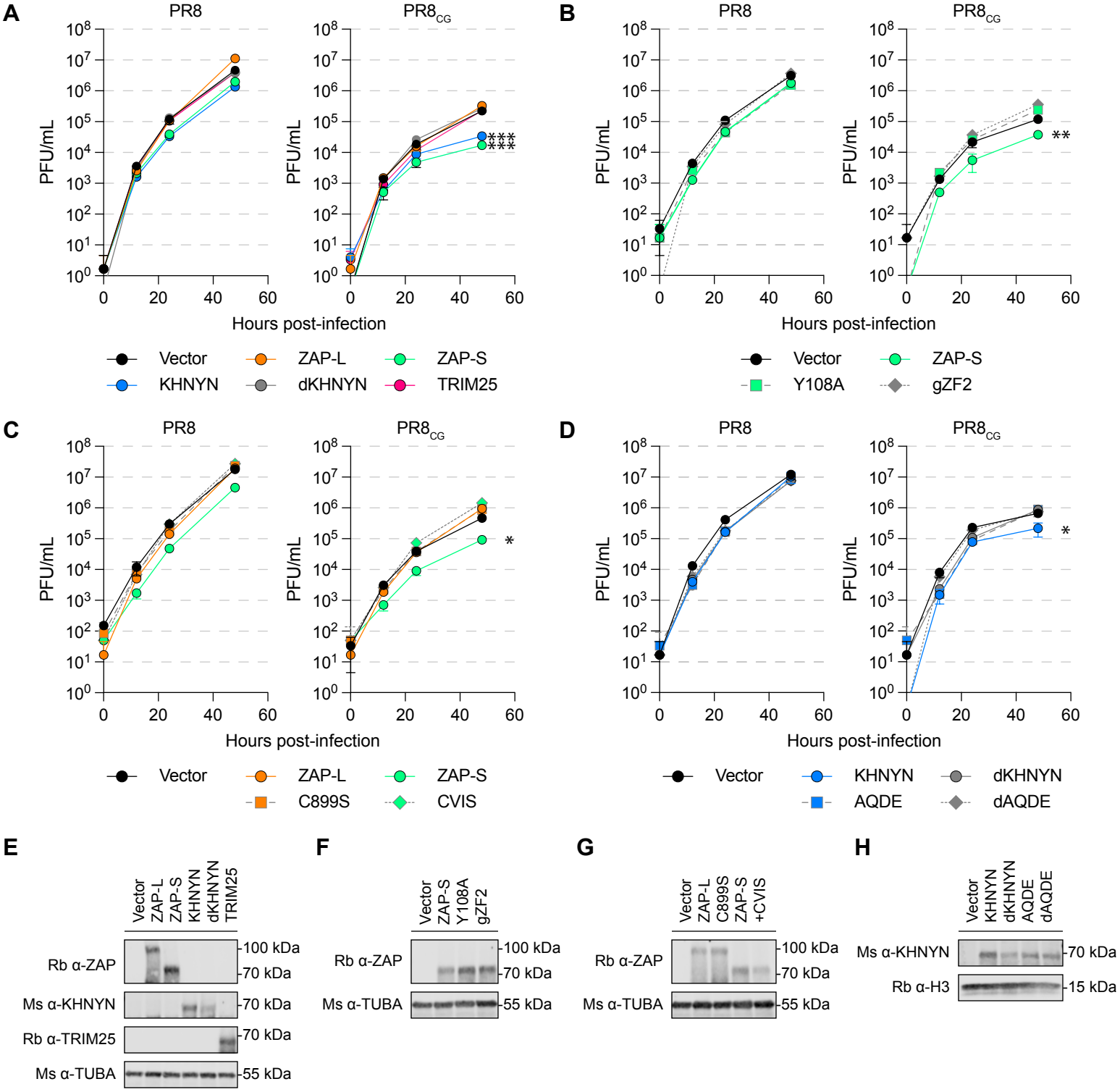
A
PR8
PR8CG
PFU/mL
Hours post-infection
***
***
Vector
KHNYN
ZAP-L
dKHNYN
ZAP-S
TRIM25
B
PR8
PR8CG
PFU/mL
Hours post-infection
**
Vector
Y108A
ZAP-S
gZF2
C
PR8
PR8CG
PFU/mL
Hours post-infection
*
Vector
C899S
ZAP-L
CVIS
ZAP-S
D
PR8
PR8CG
PFU/mL
Hours post-infection
*
Vector
AQDE
KHNYN
dKHNYN
dAQDE
E
Vector
ZAP-L
ZAP-S
KHNYN
dKHNYN
TRIM25
Rb α-ZAP
Ms α-KHNYN
Rb α-TRIM25
Ms α-TUBA
100 kDa
70 kDa
70 kDa
70 kDa
55 kDa
F
Vector
ZAP-S
Y108A
gZF2
Rb α-ZAP
Ms α-TUBA
100 kDa
70 kDa
55 kDa
G
Vector
ZAP-L
C899S
ZAP-S
+CVIS
Rb α-ZAP
Ms α-TUBA
100 kDa
70 kDa
55 kDa
H
Vector
KHNYN
dKHNYN
AQDE
dAQDE
Ms α-KHNYN
Rb α-H3
70 kDa
15 kDa

Figure 3

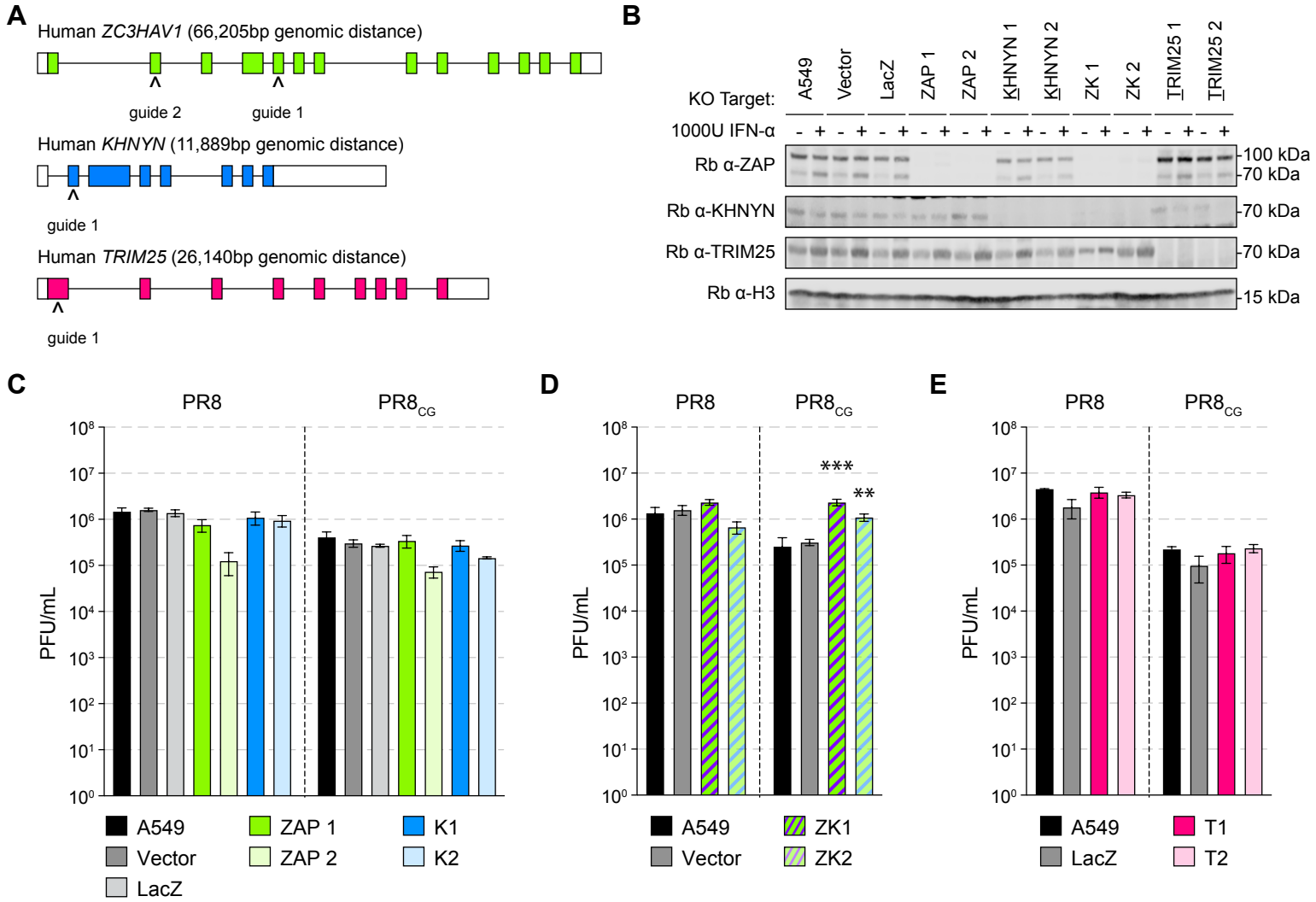
A
Human ZC3HAV1 (66,205bp genomic distance)
guide 2
guide 1
Human KHNYN (11,889bp genomic distance)
guide 1
Human TRIM25 (26,140bp genomic distance)
guide 1
B
KO Target:
A549
Vector
LacZ
ZAP 1
ZAP 2
KHNYN 1
KHNYN 2
ZK 1
ZK 2
TRIM25 1
TRIM25 2
1000U IFN-α
Rb α-ZAP
Rb α-KHNYN
Rb α-TRIM25
Rb α-H3
100 kDa
70 kDa
70 kDa
70 kDa
15 kDa
C
PR8
PR8CG
PFU/mL
A549
Vector
LacZ
ZAP 1
ZAP 2
K1
K2
D
PR8
PR8CG
***
**
PFU/mL
A549
Vector
ZK1
ZK2
E
PR8
PR8CG
PFU/mL
A549
LacZ
T1
T2

Figure 4

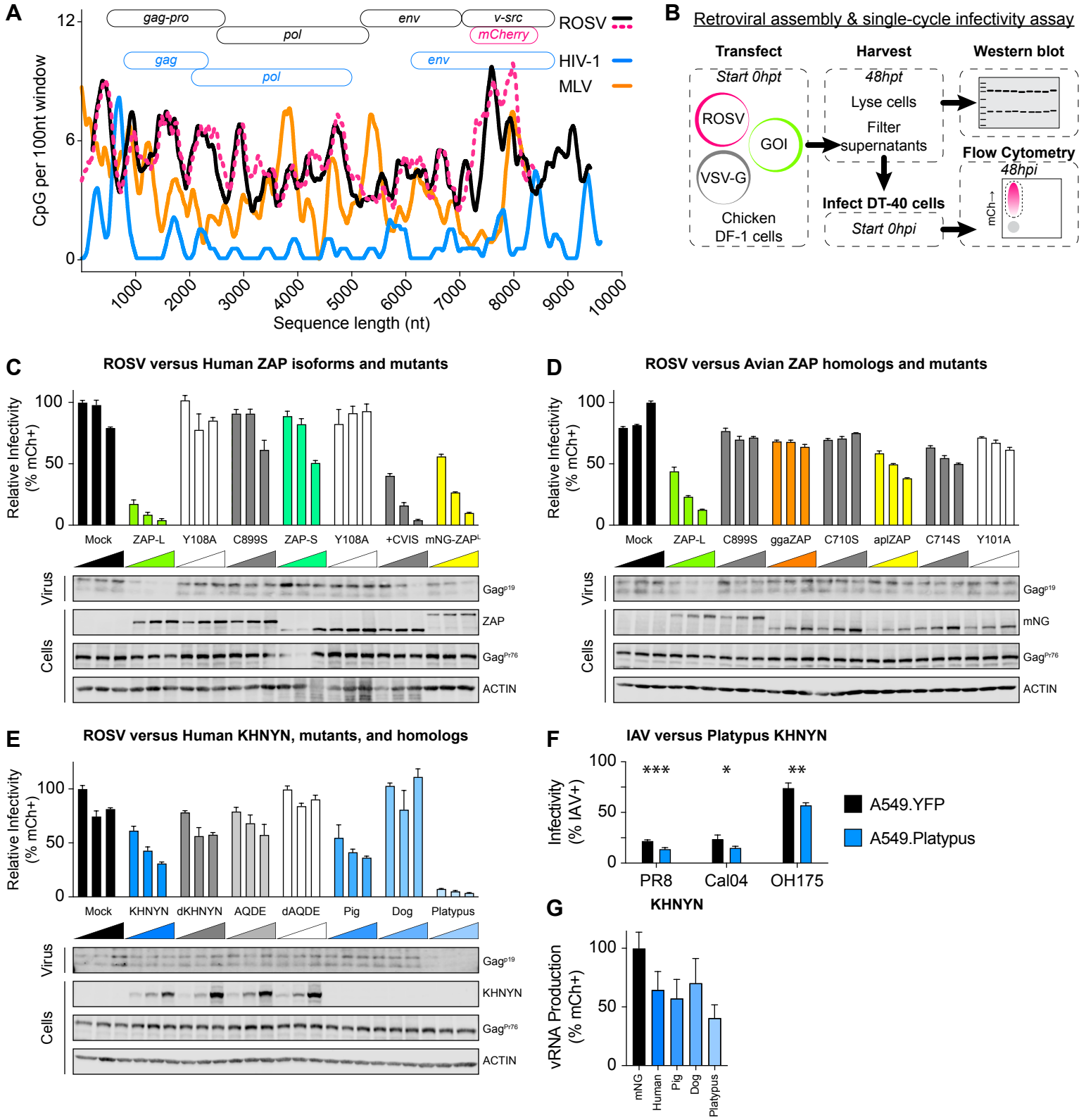
A
gag-pro
pol
env
v-src
mCherry
ROSV
gag
pol
env
HIV-1
MLV
CpG per 100nt window
Sequence length (nt)
B
Retroviral assembly & single-cycle infectivity assay
Transfect
Harvest
Western blot
Start 0hpt
ROSV
GOI
VSV-G
Chicken DF-1 cells
48hpt
Lyse cells
Filter supernatants
Infect DT-40 cells
Start 0hpi
Flow Cytometry
48hpi
mCh→
C
ROSV versus Human ZAP isoforms and mutants
Relative Infectivity (% mCh+)
Mock
ZAP-L
Y108A
C899S
ZAP-S
Y108A
+CVIS
mNG-ZAP^L
Virus
Cells
Gag^p19
ZAP
Gag^Pr76
ACTIN
D
ROSV versus Avian ZAP homologs and mutants
Relative Infectivity (% mCh+)
Mock
ZAP-L
C899S
ggaZAP
C710S
aplZAP
C714S
Y101A
Virus
Cells
Gag^p19
mNG
Gag^Pr76
ACTIN
E
ROSV versus Human KHNYN, mutants, and homologs
Relative Infectivity (% mCh+)
Mock
KHNYN
dKHNYN
AQDE
dAQDE
Pig
Dog
Platypus
Virus
Cells
Gag^p19
KHNYN
Gag^Pr76
ACTIN
F
IAV versus Platypus KHNYN
Infectivity (% IAV+)
***
*
**
PR8
Cal04
OH175
A549.YFP
A549.Platypus
G
KHNYN
vRNA Production (% mCh+)
mNG
Human
Pig
Dog
Platypus

S1 Fig

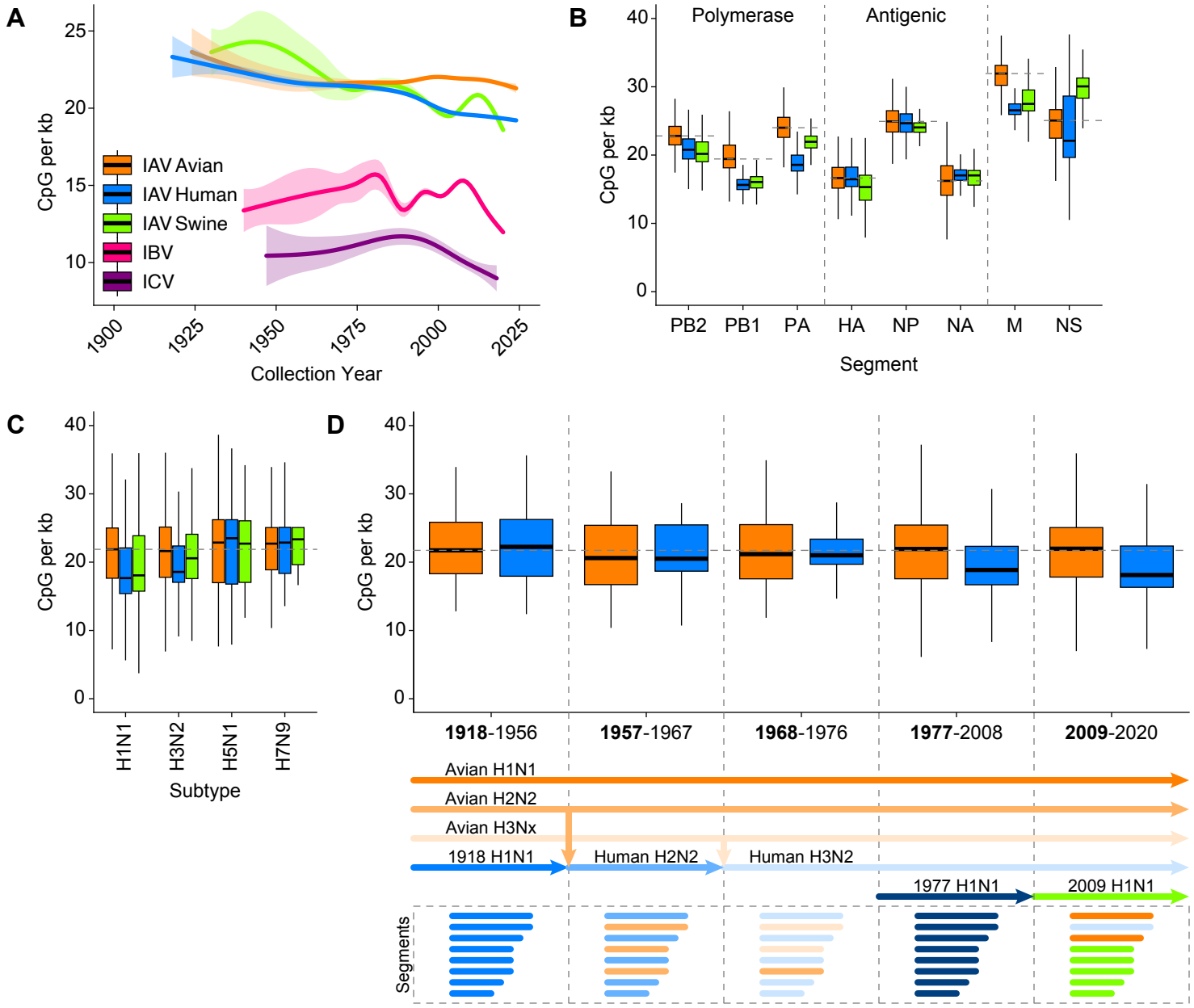
A
CpG per kb
Collection Year
IAV Avian
IAV Human
IAV Swine
IBV
ICV
B
Polymerase
Antigenic
CpG per kb
PB2
PB1
PA
HA
NP
NA
M
NS
Segment
C
CpG per kb
H1N1
H3N2
H5N1
H7N9
Subtype
D
CpG per kb
1918-1956
1957-1967
1968-1976
1977-2008
2009-2020
Avian H1N1
Avian H2N2
Avian H3Nx
1918 H1N1
Human H2N2
Human H3N2
1977 H1N1
2009 H1N1
Segments

S2 Fig

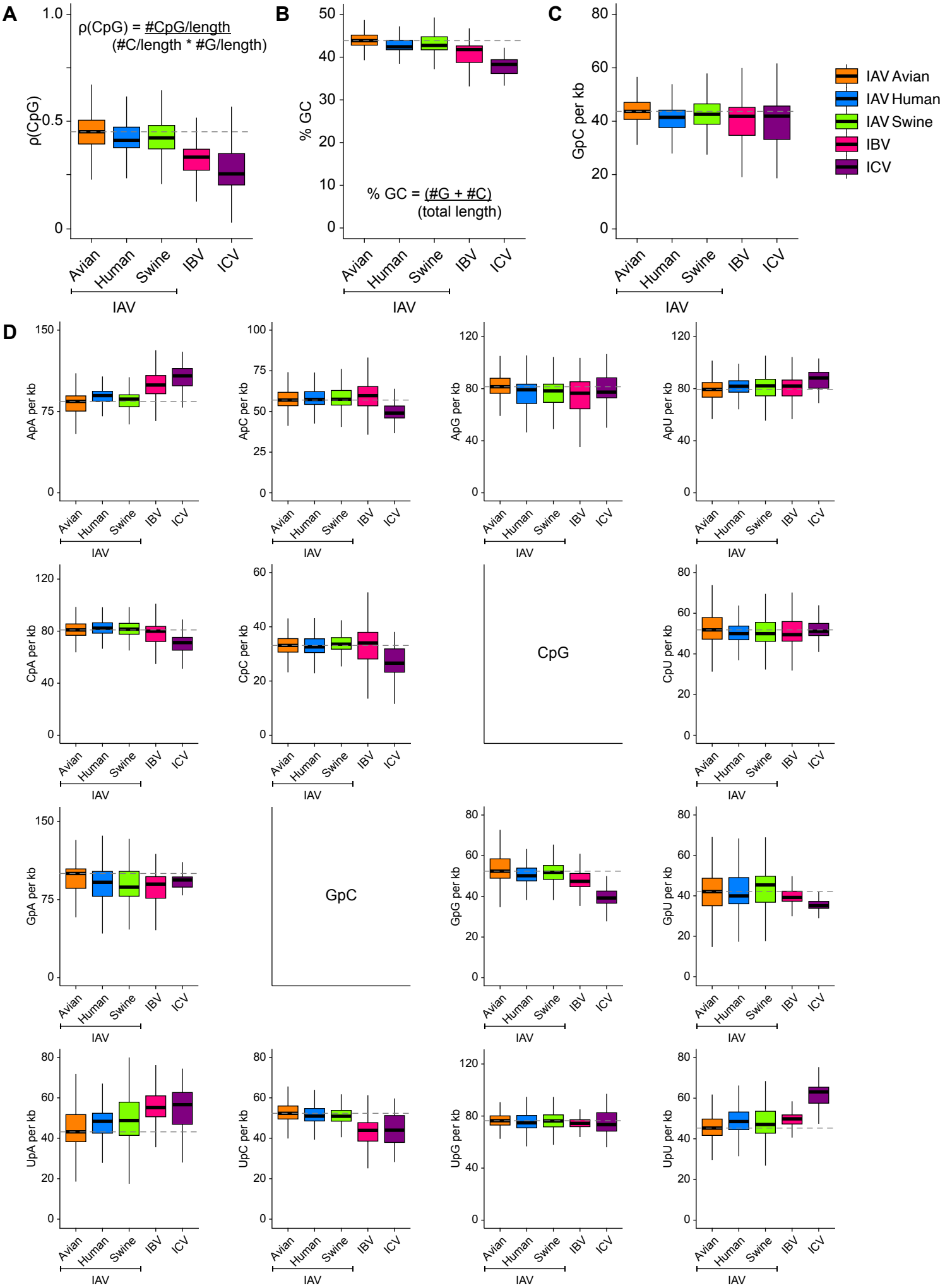
A
ρ(CpG) = #CpG/length
(#C/length * #G/length)
ρ(CpG)
B
% GC
% GC = (#G + #C)
(total length)
C
GpC per kb
IAV Avian
IAV Human
IAV Swine
IBV
ICV
Avian
Human
Swine
IBV
ICV
IAV
D
ApA per kb
ApC per kb
ApG per kb
ApU per kb
CpA per kb
CpC per kb
CpG
CpU per kb
GpA per kb
GpC
GpG per kb
GpU per kb
UpA per kb
UpC per kb
UpG per kb
UpU per kb

S3 Fig

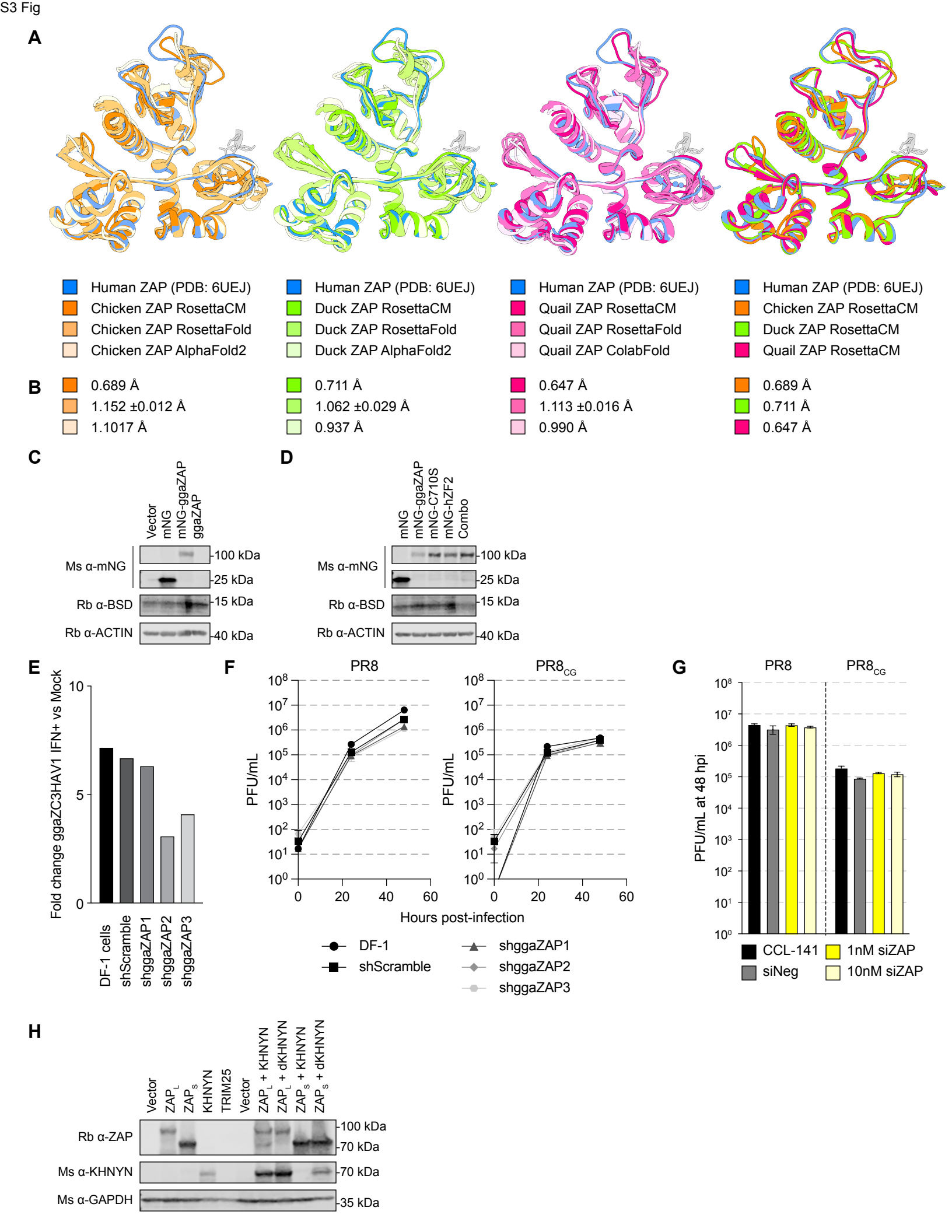
A
Human ZAP (PDB: 6UEJ)
Chicken ZAP RosettaCM
Chicken ZAP RosettaFold
Chicken ZAP AlphaFold2
Human ZAP (PDB: 6UEJ)
Duck ZAP RosettaCM
Duck ZAP RosettaFold
Duck ZAP AlphaFold2
Human ZAP (PDB: 6UEJ)
Quail ZAP RosettaCM
Quail ZAP RosettaFold
Quail ZAP ColabFold
Human ZAP (PDB: 6UEJ)
Chicken ZAP RosettaCM
Duck ZAP RosettaCM
Quail ZAP RosettaCM
B
0.689 Å
1.152 ±0.012 Å
1.1017 Å
0.711 Å
1.062 ±0.029 Å
0.937 Å
0.647 Å
1.113 ±0.016 Å
0.990 Å
0.689 Å
0.711 Å
0.647 Å
C
Vector
mNG
mNG-ggaZAP
ggaZAP
Ms α-mNG
Rb α-BSD
Rb α-ACTIN
100 kDa
25 kDa
15 kDa
40 kDa
D
mNG
mNG-ggaZAP
mNG-C710S
mNG-hZF2
Combo
Ms α-mNG
Rb α-BSD
Rb α-ACTIN
100 kDa
25 kDa
15 kDa
40 kDa
E
Fold change ggaZC3HAV1 IFN+ vs Mock
DF-1 cells
shScramble
shggaZAP1
shggaZAP2
shggaZAP3
F
PR8
PR8CG
PFU/mL
Hours post-infection
DF-1
shScramble
shggaZAP1
shggaZAP2
shggaZAP3
G
PR8
PR8CG
PFU/mL at 48 hpi
CCL-141
siNeg
1nM siZAP
10nM siZAP
H
Vector
ZAPL
ZAPS
KHNYN
TRIM25
Vector
ZAPL + KHNYN
ZAPL + dKHNYN
ZAPS + KHNYN
ZAPS + dKHNYN
Rb α-ZAP
Ms α-KHNYN
Ms α-GAPDH
100 kDa
70 kDa
70 kDa
35 kDa

S4 Fig

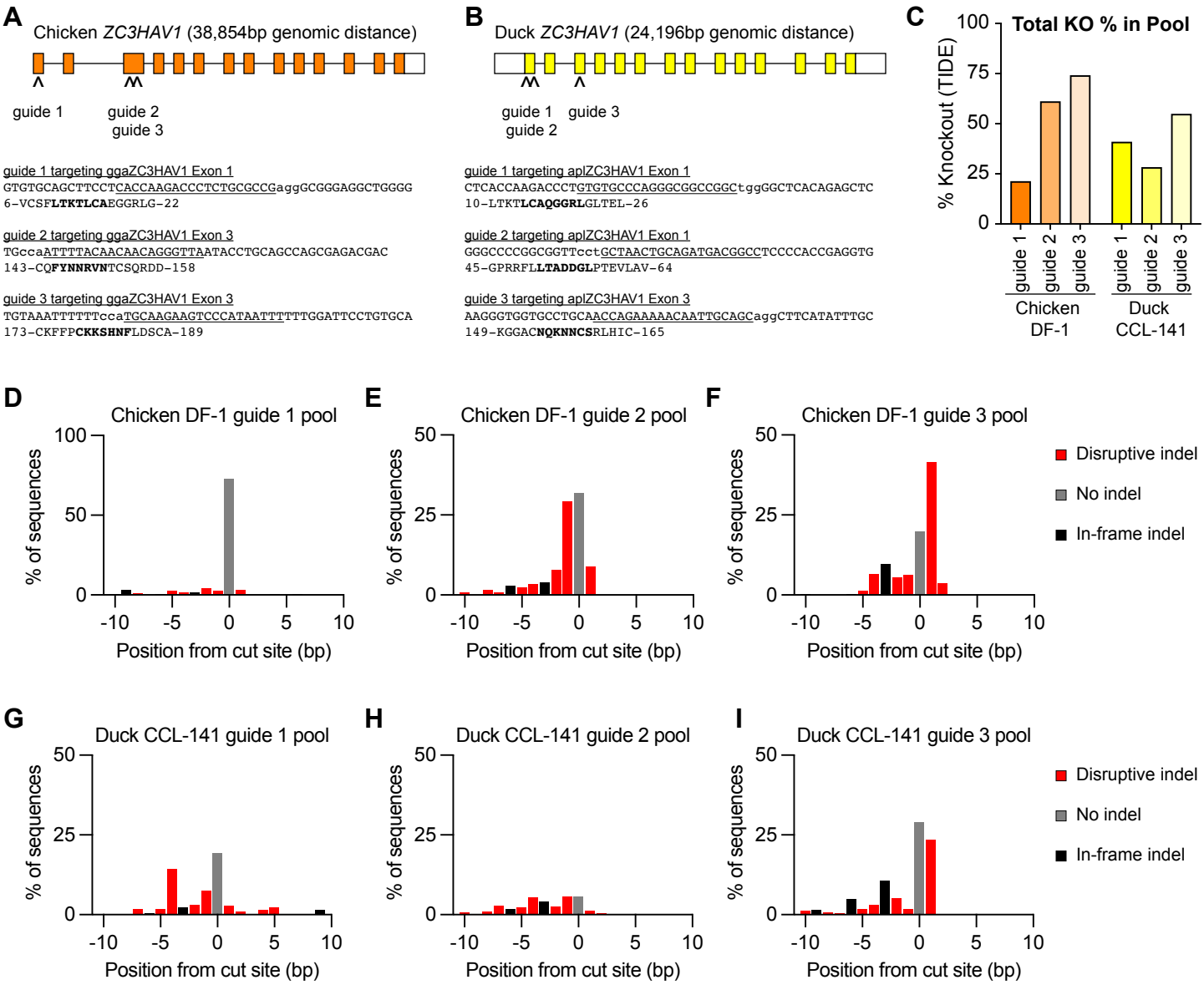
A
Chicken ZC3HAV1 (38,854bp genomic distance)
guide 1
guide 2
guide 3
guide 1 targeting ggaZC3HAV1 Exon 1
GTGTGCAGCTTCCTCACCAAGACCCTCTGCGCCGaggGCGGGAGGCTGGGG
6-VCSFLTKTLCAEGGRLG-22
guide 2 targeting ggaZC3HAV1 Exon 3
TGccaATTTTACAACAACAGGGTTAATACCTGCAGCCAGCGAGACGAC
143-CQFYNNRVNTCSQRDD-158
guide 3 targeting ggaZC3HAV1 Exon 3
TGTAAATTTTTTccaTGCAAGAAGTCCCATAATTTTTTGGATTCCTGTGCA
173-CKFFPCKKSHNFLDSCA-189
B
Duck ZC3HAV1 (24,196bp genomic distance)
guide 1
guide 2
guide 3
guide 1 targeting aplZC3HAV1 Exon 1
CTCACCAAGACCCTGTGTGCCCAGGGCGGCCGGCtggGGCTCACAGAGCTC
10-LTKTLCAQGGRLGLTEL-26
guide 2 targeting aplZC3HAV1 Exon 1
GGGCCCCGGCGGTTcctGCTAACTGCAGATGACGGCCTCCCCACCGAGGTG
45-GPRRFLLTADDGLPTEVLAV-64
guide 3 targeting aplZC3HAV1 Exon 3
AAGGGTGGTGCCTGCAACCAGAAAAACAATTGCAGCaggCTTCATATTTGC
149-KGGACNQKNNCSRLHIC-165
C
Total KO % in Pool
% Knockout (TIDE)
100
75
50
25
0
guide 1
guide 2
guide 3
guide 1
guide 2
guide 3
Chicken DF-1
Duck CCL-141
D
Chicken DF-1 guide 1 pool
E
Chicken DF-1 guide 2 pool
F
Chicken DF-1 guide 3 pool
% of sequences
Position from cut site (bp)
Disruptive indel
No indel
In-frame indel
G
Duck CCL-141 guide 1 pool
H
Duck CCL-141 guide 2 pool
I
Duck CCL-141 guide 3 pool

S5 Fig

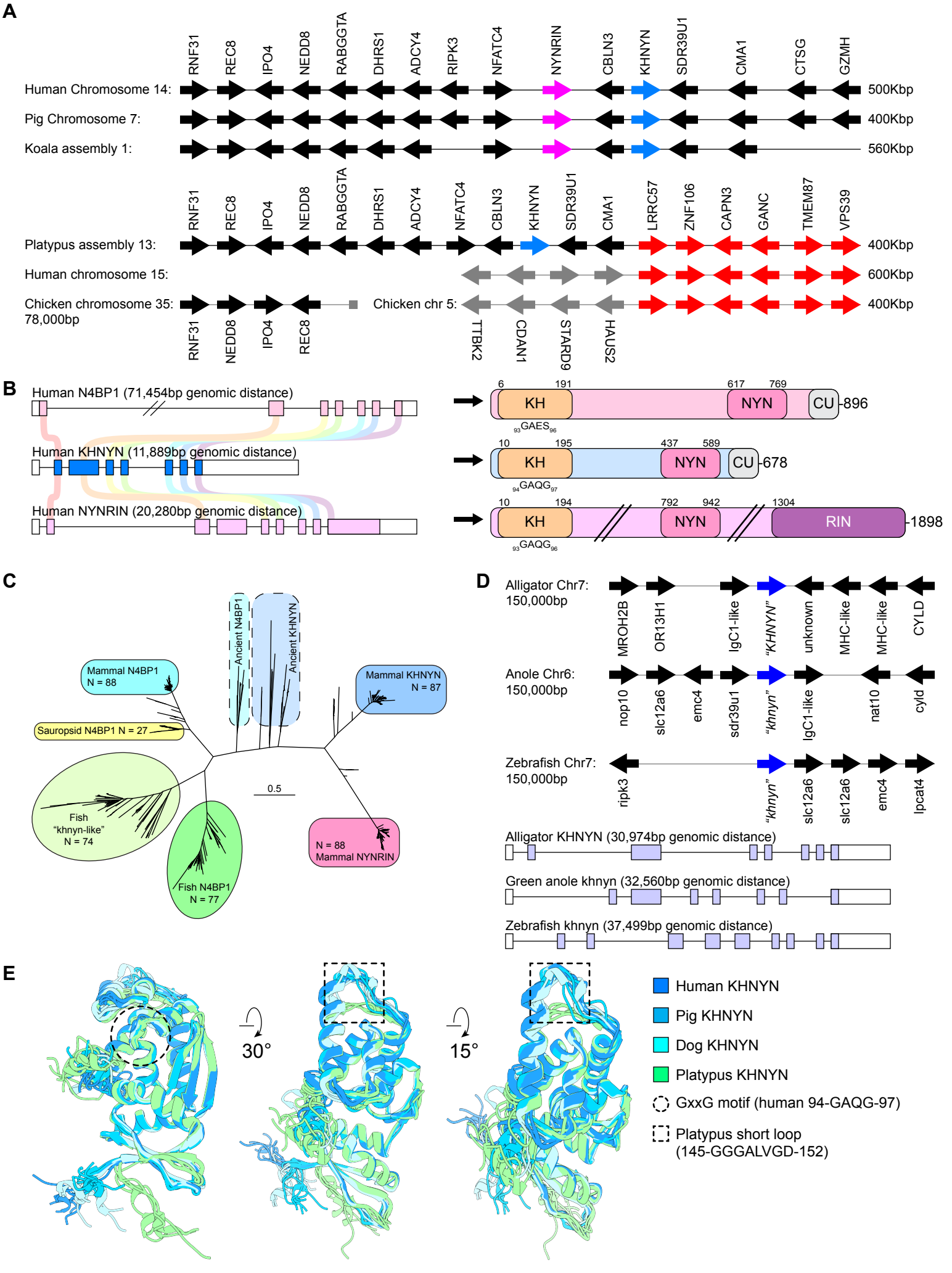
A
RNF31
REC8
IPO4
NEDD8
RABGGTA
DHRS1
ADCY4
RIPK3
NFATC4
NYNRIN
CBLN3
KHNYN
SDR39U1
CMA1
CTSG
GZMH
Human Chromosome 14:
500Kbp
Pig Chromosome 7:
400Kbp
Koala assembly 1:
560Kbp
RNF31
REC8
IPO4
NEDD8
RABGGTA
DHRS1
ADCY4
NFATC4
CBLN3
KHNYN
SDR39U1
CMA1
LRRC57
ZNF106
CAPN3
GANC
TMEM87
VPS39
Platypus assembly 13:
400Kbp
Human chromosome 15:
600Kbp
Chicken chromosome 35:
78,000bp
Chicken chr 5:
400Kbp
RNF31
NEDD8
IPO4
REC8
TTBK2
CDAN1
STARD9
HAUS2
B
Human N4BP1 (71,454bp genomic distance)
Human KHNYN (11,889bp genomic distance)
Human NYNRIN (20,280bp genomic distance)
6
191
617
769
KH
NYN
CU
896
93GAES96
10
195
437
589
KH
NYN
CU
678
94GAQG97
10
194
792
942
1304
KH
NYN
RIN
1898
93GAQG96
C
Ancient N4BP1
Ancient KHNYN
Mammal N4BP1
N = 88
Mammal KHNYN
N = 87
Sauropsid N4BP1 N = 27
0.5
Fish
"khnyn-like"
N = 74
Fish N4BP1
N = 77
N = 88
Mammal NYNRIN
D
Alligator Chr7:
150,000bp
MROH2B
OR13H1
IgC1-like
"KHNYN"
unknown
MHC-like
MHC-like
CYLD
Anole Chr6:
150,000bp
nop10
slc12a6
emc4
sdr39u1
"khnyn"
IgC1-like
nat10
cyld
Zebrafish Chr7:
150,000bp
ripk3
"khnyn"
slc12a6
slc12a6
emc4
lpcat4
Alligator KHNYN (30,974bp genomic distance)
Green anole khnyn (32,560bp genomic distance)
Zebrafish khnyn (37,499bp genomic distance)
E
30°
15°
Human KHNYN
Pig KHNYN
Dog KHNYN
Platypus KHNYN
GxxG motif (human 94-GAQG-97)
Platypus short loop
(145-GGGALVGD-152)

S6 Fig

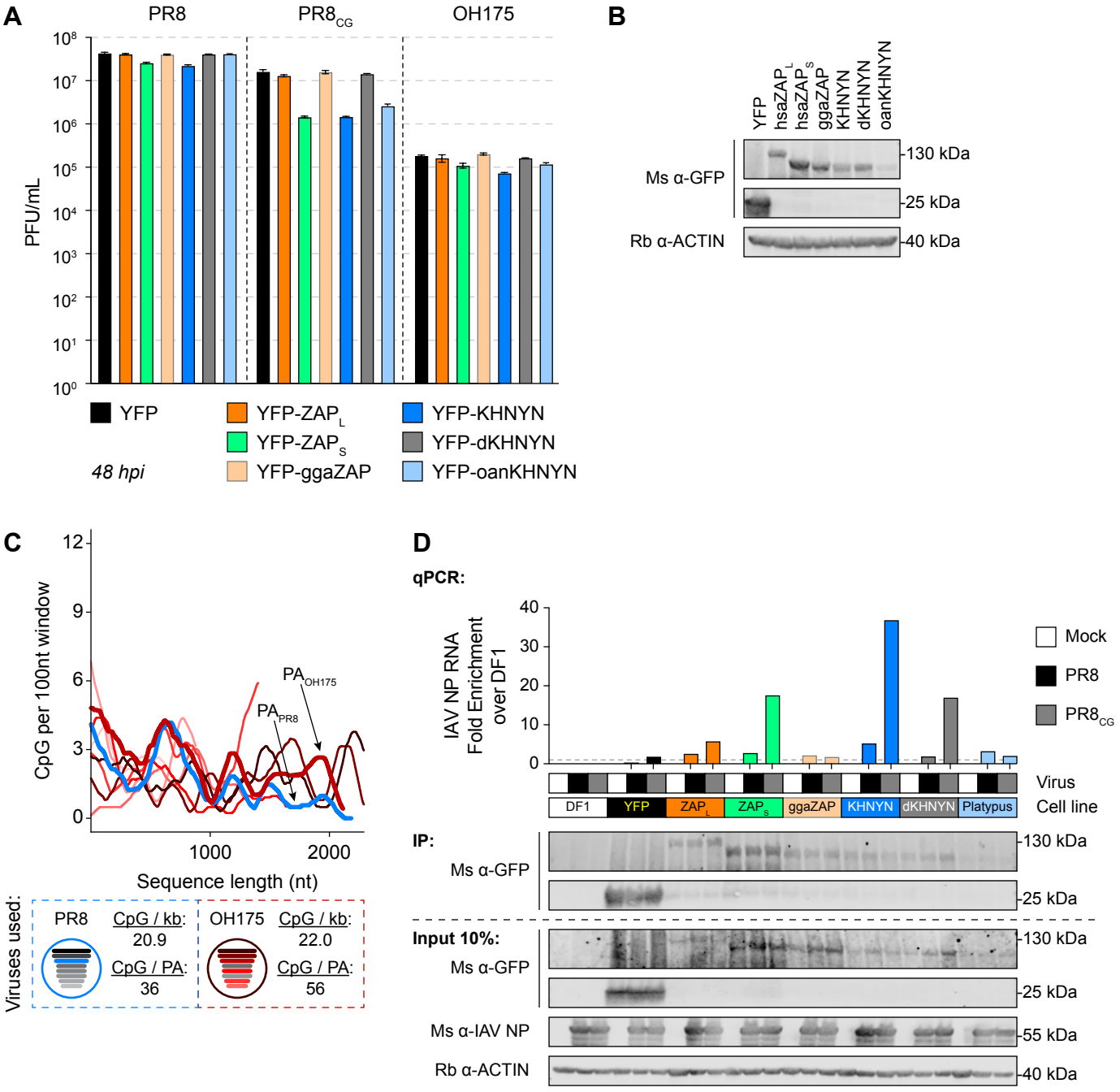
A
PR8
PR8CG
OH175
PFU/mL
YFP
YFP-ZAPL
YFP-ZAPS
YFP-ggaZAP
YFP-KHNYN
YFP-dKHNYN
YFP-oanKHNYN
48 hpi
B
YFP
hsaZAPL
hsaZAPS
ggaZAP
KHNYN
dKHNYN
oanKHNYN
Ms α-GFP
Rb α-ACTIN
130 kDa
25 kDa
40 kDa
C
CpG per 100nt window
PAOH175
PAPR8
Sequence length (nt)
Viruses used:
PR8
CpG / kb: 20.9
CpG / PA: 36
OH175
CpG / kb: 22.0
CpG / PA: 56
D
qPCR:
IAV NP RNA Fold Enrichment over DF1
Mock
PR8
PR8CG
Virus
Cell line
DF1
YFP
ZAPL
ZAPS
ggaZAP
KHNYN
dKHNYN
Platypus
IP:
Ms α-GFP
Input 10%:
Ms α-IAV NP
Rb α-ACTIN
130 kDa
25 kDa
55 kDa
40 kDa

S7 Fig

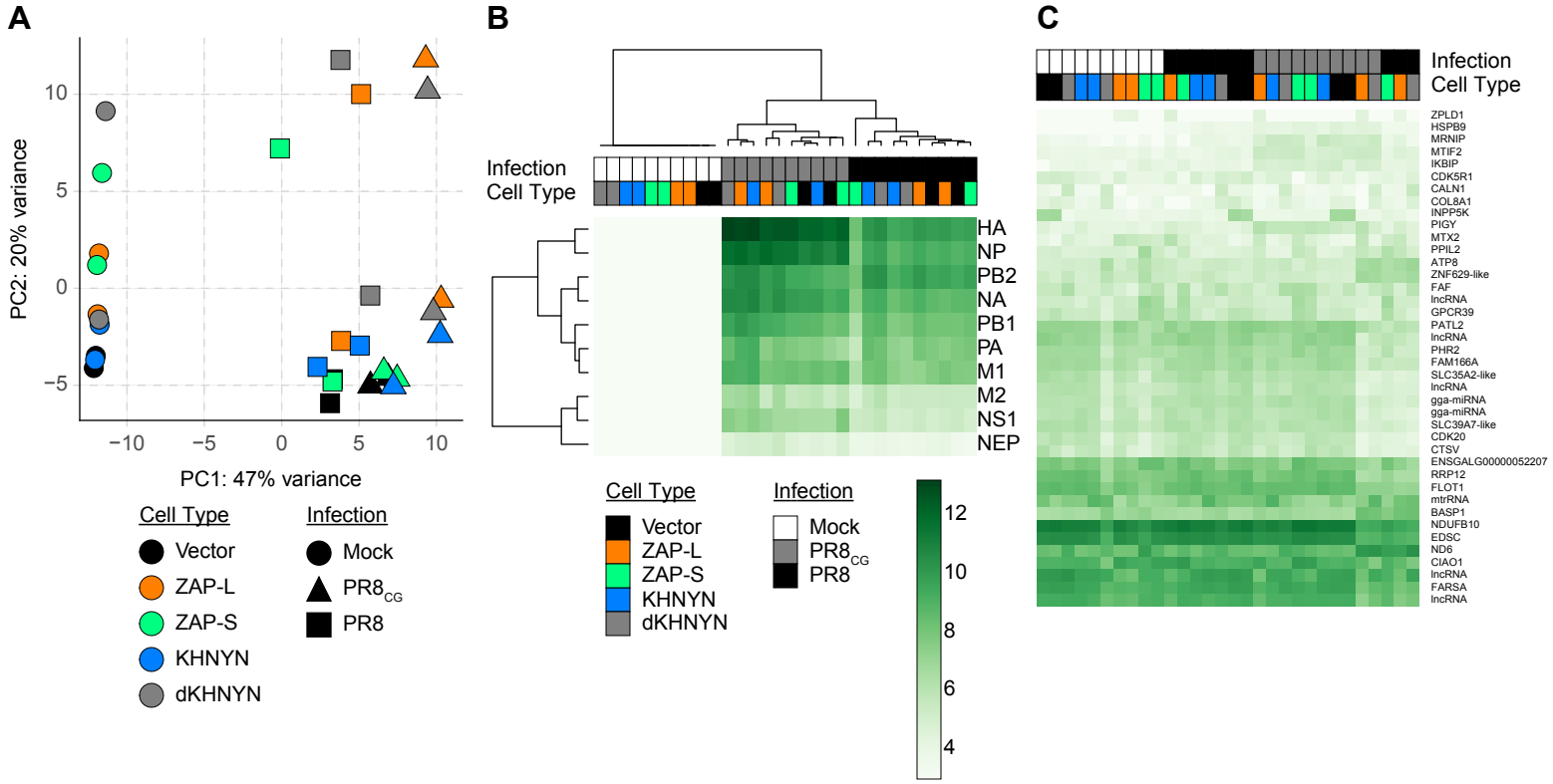
A
PC2: 20% variance
PC1: 47% variance
10
5
0
−5
−10
−5
0
5
10
Cell Type
Vector
ZAP-L
ZAP-S
KHNYN
dKHNYN
Infection
Mock
PR8CG
PR8
B
Infection
Cell Type
HA
NP
PB2
NA
PB1
PA
M1
M2
NS1
NEP
Cell Type
Vector
ZAP-L
ZAP-S
KHNYN
dKHNYN
Infection
Mock
PR8CG
PR8
12
10
8
6
4
C
Infection
Cell Type
ZPLD1
HSPB9
MRNIP
MTIF2
IKBIP
CDK5R1
CALN1
COL8A1
INPP5K
PIGY
MTX2
PPIL2
ATP8
ZNF629-like
FAF
lncRNA
GPCR39
PATL2
lncRNA
PHR2
FAM166A
SLC35A2-like
lncRNA
gga-miRNA
gga-miRNA
SLC39A7-like
CDK20
CTSV
ENSGALG00000052207
RRP12
FLOT1
mtrRNA
BASP1
NDUFB10
EDSC
ND6
CIAO1
lncRNA
FARSA
lncRNA

S8 Fig

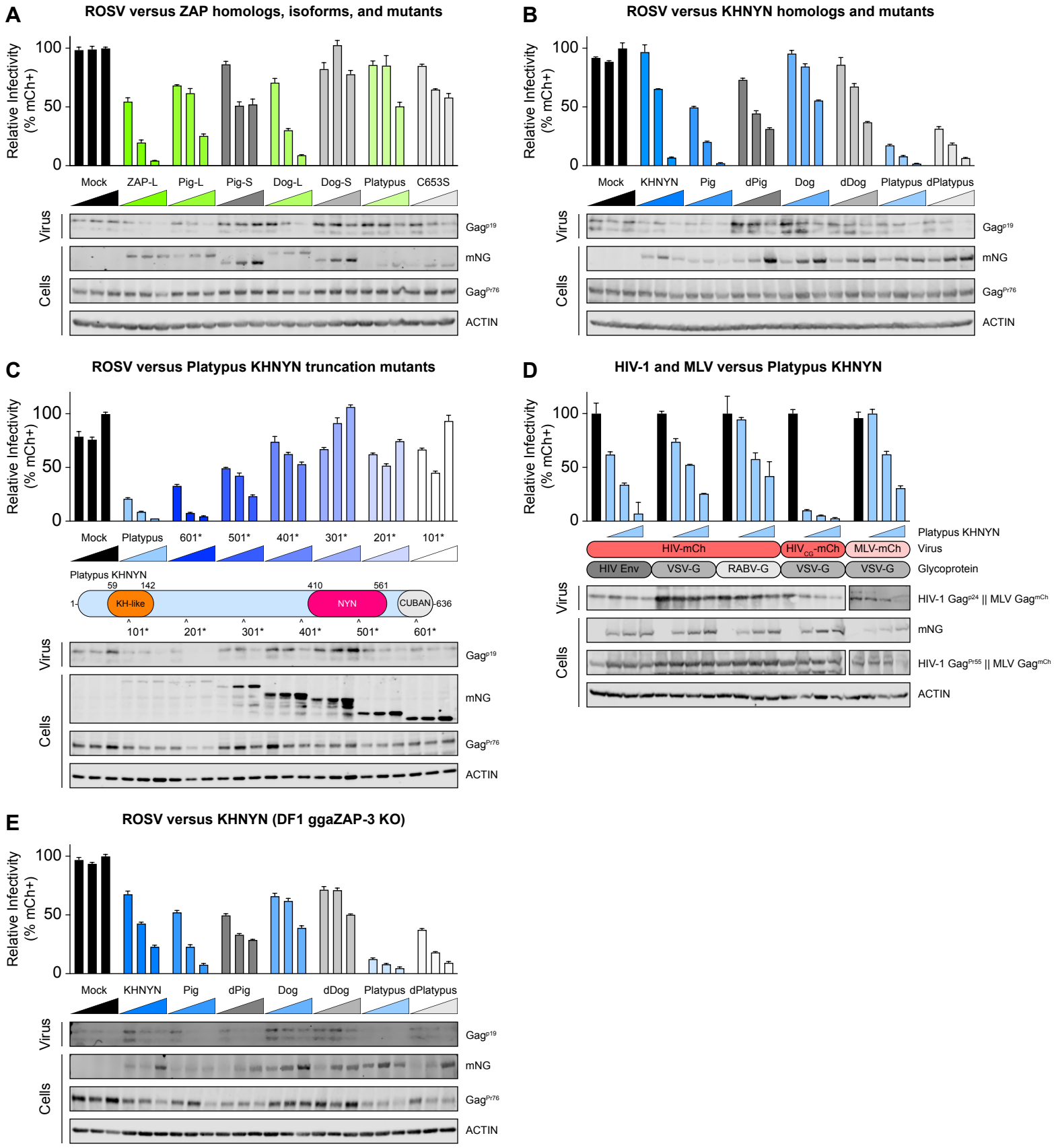
A
ROSV versus ZAP homologs, isoforms, and mutants
Relative Infectivity (% mCh+)
100
50
0
Mock
ZAP-L
Pig-L
Pig-S
Dog-L
Dog-S
Platypus
C653S
Virus
Cells
Gag p19
mNG
Gag Pr76
ACTIN
B
ROSV versus KHNYN homologs and mutants
Mock
KHNYN
Pig
dPig
Dog
dDog
Platypus
dPlatypus
C
ROSV versus Platypus KHNYN truncation mutants
Mock
Platypus
601*
501*
401*
301*
201*
101*
Platypus KHNYN
59
142
410
561
1-
KH-like
NYN
CUBAN
-636
D
HIV-1 and MLV versus Platypus KHNYN
Platypus KHNYN
HIV-mCh
HIV CG -mCh
MLV-mCh
Virus
HIV Env
VSV-G
RABV-G
VSV-G
VSV-G
Glycoprotein
HIV-1 Gag p24 || MLV Gag mCh
HIV-1 Gag Pr55 || MLV Gag mCh
E
ROSV versus KHNYN (DF1 ggaZAP-3 KO)

S9 Fig

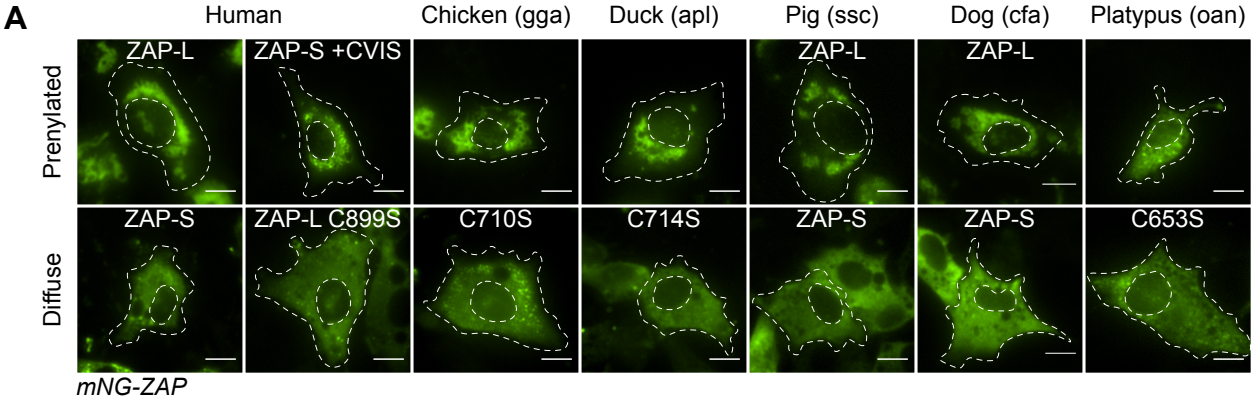

B

Human	CVIS*
Chimpanzee	....
Pig	....
Dog	....
Cat	....
Horse	....
Mouse	.I..
Rat	.I..
Platypus	.NLQ
Chicken	.IVC
Quail	.IV.
Duck	.I..

S10 Fig

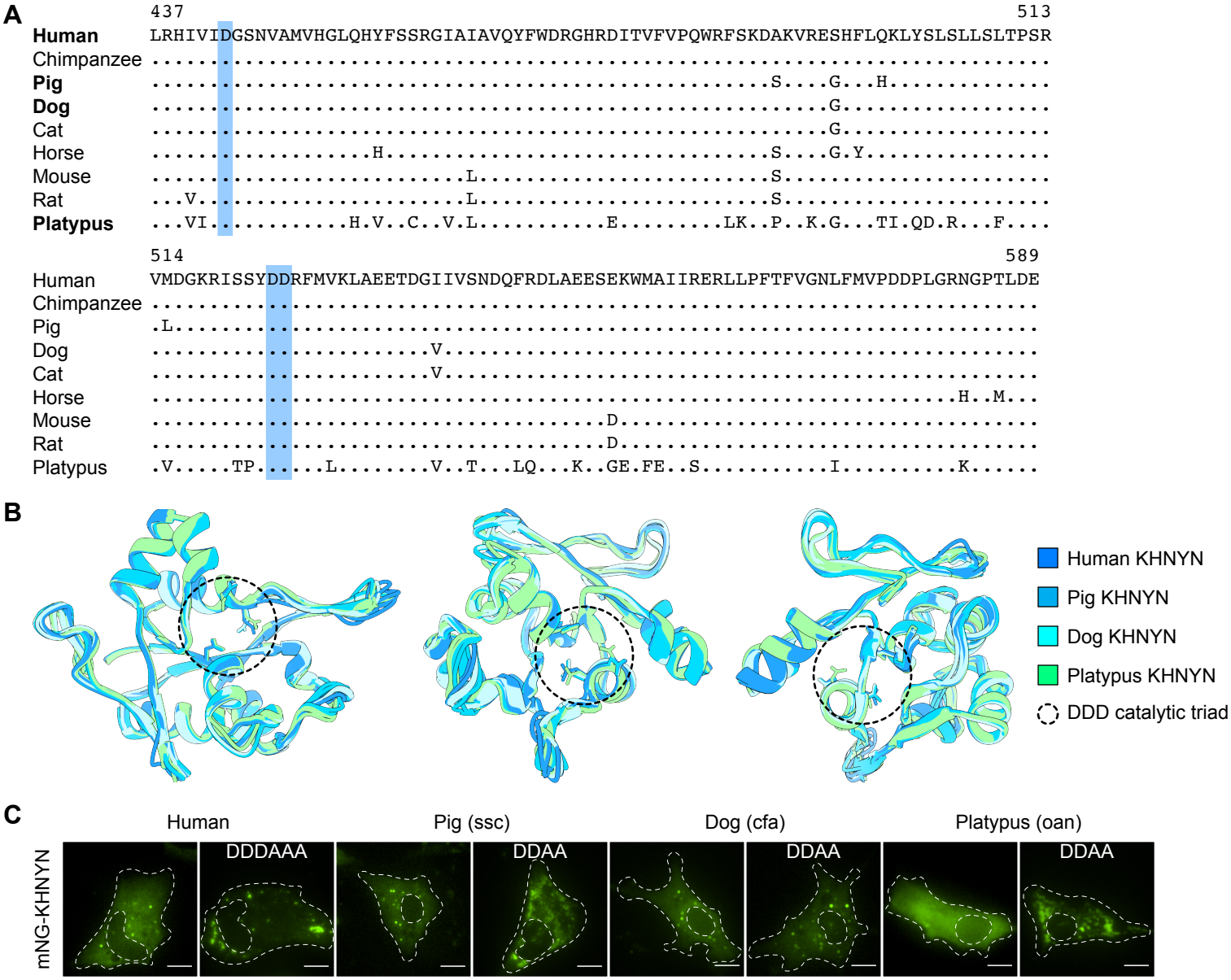
A
437
513
Human LRHIVIDGSNVAMVHGLQHYFSSRGIAIAVQYFWDRGHRDITVFVPQWRFSKDAKVRESHFLQKLYSLSLLSLTPSR
Chimpanzee
Pig
Dog
Cat
Horse
Mouse
Rat
Platypus
514
589
Human VMDGKRISSYDDRFMVKLAEETDGIIVSNDQFRDLAEESEKWMAIIRERLLPFTFVGNLFMVPDDPLGRNGPTLDE
Chimpanzee
Pig
Dog
Cat
Horse
Mouse
Rat
Platypus
B
Human KHNYN
Pig KHNYN
Dog KHNYN
Platypus KHNYN
DDD catalytic triad
C
Human
Pig (ssc)
Dog (cfa)
Platypus (oan)
mNG-KHNYN
DDDAAA
DDAA
DDAA
DDAA